ACS MEASUREMENT SCIENCE Au
AN OPEN ACCESS JOURNAL OF THE AMERICAN CHEMICAL SOCIETY

pubs.acs.org/measureau
Article

Molecular-Level Characterization of Carbonaceous Aerosols via Coupled Thermal-Optical Carbon Analysis and Ultra-High-Resolution FT-ICR Mass Spectrometry

Silvia Juliana Vesga-Martínez, Christopher Paul Rüger,* Fabian Etscheidt, Martin Bauer, Patrick Martens, Anika Neumann, Hendryk Czech, and Ralf Zimmermann

Cite This: https://doi.org/10.1021/acsmeasuresciau.5c00170
Read Online

ACCESS | Metrics & More | Article Recommendations | Supporting Information

ABSTRACT: Comprehensive molecular-level characterization of carbonaceous aerosols is essential for understanding their environmental transformations, optical properties, and health effects. Here, we present a hyphenated analytical approach combining a thermal-optical carbon analyzer (TOCA) with atmospheric pressure photoionization Fourier transform ion cyclotron resonance mass spectrometry (APPI-FT-ICR-MS) for the direct, temperature-resolved molecular analysis of particulate matter (PM). The method enables the simultaneous quantification and chemical speciation of evolved organic and elemental carbon fractions, following the IMPROVE_A protocol, thereby distinguishing between organic and elemental carbon fractions. The system achieves subppm mass accuracy and resolving power exceeding 2.6 × 10^5 at m/z 400, ensuring reliable differentiation of critical mass splits such as C_3 vs SH_4 (3.4 mDa) and allowing the unambiguous assignment of thousands of sum formulas across complex aerosol matrices. Compared with resonance-enhanced multiphoton ionization time-of-flight MS, the APPI-FT-ICR-MS coupling expands the accessible chemical space toward oxygenated and sulfur-containing species while maintaining robust performance and reproducibility. Application to representative aerosol sources, including ship diesel emissions, residential wood combustion, and ambient PM from Beijing, demonstrated distinct molecular fingerprints. Ship emissions were dominated by CH- and CHS-class species with double bond equivalents (DBE) ≤20, indicative of alkylated polycyclic aromatics, whereas wood combustion particles contained more oxidized CHO- and CHNO-classes with enhanced aromaticity and nitrogen incorporation. Ambient aerosols exhibited mixed signatures with elevated OC/EC ratios (∼3−4) and high contributions from oxygenated and nitrate-bearing compounds, reflecting secondary formation and seasonal variability. This integrated TOCA-APPI-FT-ICR-MS approach provides unprecedented resolution of thermally evolved aerosol species, bridging operational OC/EC quantification with molecular-level speciation. By correlating volatility, aromaticity, and oxidation state across source types, it establishes a powerful framework for tracing aerosol origins, transformation processes, and their environmental and health relevance.

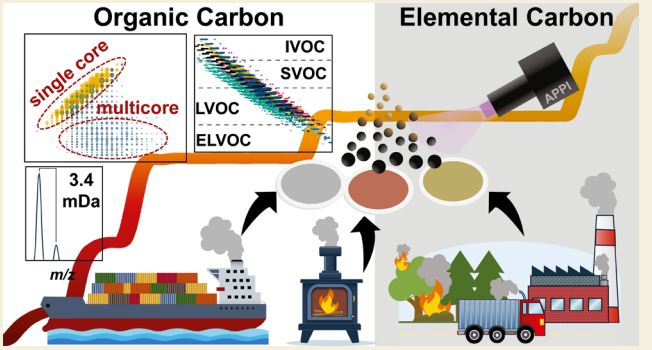

KEYWORDS: *thermal-optical carbon analyzer, high-resolution mass spectrometry, carbonaceous aerosols, atmospheric pressure photoionization, particulate matter*

1. INTRODUCTION

Airborne particulate matter (PM) strongly influences climate-relevant atmospheric processes and causes adverse cardiovascular and respiratory health effects.[1,2] A key contributor to these impacts is the carbonaceous fraction of PM, which plays a central role in determining chemical reactivity, optical properties (e.g., light absorption), and cloud formation. A differentiation into organic carbon (OC), i.e., the carbon of all organic species contained in PM, or elemental carbon (EC), e.g., soot and char particles, often serve as a diagnostic metric for PM source apportionment and emission characterization.[3,4] These bulk data can routinely be retrieved from commercialized thermal-optical carbon analyzers (TOCA).

Molecular-level information on the OC fraction is essential for an in-depth understanding of molecular composition, potential sources, and transformation pathways of aerosols in

Received: November 3, 2025
Revised: January 7, 2026
Accepted: January 8, 2026

the environment. This aim is classically pursued with aerosol extracts with diverse analytical approaches, primarily chromatography and mass spectrometry. The required extraction protocols have to be tailored to the target chemistry and are often time-consuming, extensively consuming sample material, tedious, and error-prone. Consequently, direct analysis by thermal evaporation protocols coupled to a mass spectrometer has been developed as an alternative.[5] Here, a controlled temperature protocol results in the evaporation of intact molecules at lower temperatures (thermodesorption phase), whereas at elevated temperatures, intended analytical pyrolysis causes thermal fragmentation, generating diagnostic degradation products (pyrolysis phase). However, direct inlet probe (DIP)[6] or atmospheric solid analysis probe (ASAP),[7,8] lack the capability for bulk fraction classification and often have low repeatability and robustness.[9] Thermogravimetry, giving access to temperature-resolved quantitative mass loss data, often comes short in terms of sensitivity when applied to typical low-volume PM samples, where only μg-level loading is available.[10] TOCA, on the other hand, provides a controlled thermal desorption profile enabling an operational definition of OC and EC. The IMPROVE_A protocol, one of the most widely used standards in TOCA, results in four OC fractions: OC1 up to 140 °C, OC2 up to 280 °C, OC3 up to 480 °C, and OC4 up to 580 °C (all in inert helium atmosphere).[11] Here, OC1 and OC2 can be considered the thermodesorption phase, whereas the elevated temperatures of OC3 and OC4 will cause substantial pyrolysis. Online measurement of a negligible aliquot of the emitted material can retrieve additional molecular information. This has so far been commonly realized by coupling to universal single photon ionization (SPI) or aromatic-selective resonance-enhanced multiphoton ionization (REMPI) Time of Flight MS (ToF-MS).[4,12,13]

Annotation and identification of compounds by TOCA with SPI/REMPI-ToF-MS is largely based on a combination of a comparison with characteristics from measured samples, ionization selectivity, and in-spectra pattern analysis, e.g., alkylation homologue series, in an expert judgment manner. High-resolution mass spectrometry (HRMS) increases the confidence in environmental analysis as exact masses are gained with subppm accuracy, allowing for direct access to the molecular composition by attribution of sum formulas. Thus, the spectral information can be automatically processed, reducing manual interaction and error-prone interference. High-resolution mass spectrometers are often equipped with atmospheric pressure ionization sources, which offer higher operational robustness, simplicity, and easier access. In this respect, also photoionization-based concepts, such as atmospheric pressure photo and laser ionization (APPI/APLI), which borrow many conceptual similarities from SPI and REMPI, have been introduced and widely studied.[14−16] APPI with Krypton plasma discharge lamps emitting radiation at 10/10.6 eV for ionization is most widely used, cost-effective and has little safety concerns.[15]

In this study, the concept of understanding aerosol chemistry based on the components released during thermal optical carbon analysis is substantially expanded. We present the molecular-level analysis of the emitted carbonaceous compounds by ultra-high-resolution mass spectrometry (FT-ICR-MS) equipped with APPI. Our motivation is to overcome analytical constraints given by the commonly deployed unit mass-resolving mass analyzers by means of high mass resolution, high mass accuracy, and a high dynamic range, all while simultaneously having a robust and easy-constructed atmospheric ionization setup. Particularly, APPI has been chosen here as a low-fragmentation technique with a broad coverage of the chemical space and minimal matrix effects. Questions addressed have been the trade-offs between resolving power and acquisition speed in FT-ICR-MS, repeatability, molecular coverage, and comparative performance with established vacuum photoionization techniques, such as REMPI-ToF-MS. Finally, to assess the practical applicability of our approach, we analyzed a diverse set of real-world aerosol samples, including primary engine emissions, biomass combustion particles, and ambient aerosols.

2. MATERIALS AND METHODS

2.1. Sample Material

In this study, three sets of particulate matter samples have been investigated to encompass a wide range of chemical characteristics, representing different emission sources: marine diesel engine emissions, residential biomass combustion, and ambient aerosols (Table S1).

The first sample set focused on primary emissions from a research ship-diesel engine (four-stroke, one cylinder, maximum rated power output 80 kW) described in detail elsewhere.[17] All engine-emission samples analyzed here were collected at an engine load of 60 kW (75%), mimicking steady at-sea cruising conditions, using different fuels: an ultra-low-sulfur heavy fuel oil (ULS-HFO; 0.06 w-% S), a high-sulfur heavy fuel oil (HS-HFO; 2.4 w-% S), and marine gas oil (MGO).[18] Common emissions of residential wood combustion are covered by the analysis of primary combustion from a masonry heater fed with beech logwood.[19] The third sample set was designed to reflect actual environmental conditions and included ambient particulate matter collected during a (seasonal variation of PM) campaign in 2010/2011 at the campus of the China University of Geosciences (Beijing).[20,21]

Particulate matter was collected on quartz fiber filters (QFF, 47 mm, Whatman, USA) that had been prebaked for 6 h at 550 °C. After collection, these filters were stored in Petri dishes (Analyslide, Pall Corporation, 600 South Wagner Road, Ann Arbor, USA) at −18 °C until analysis. An exception was the Beijing samples, which were collected using high-volume samplers equipped with 150 mm diameter quartz fiber filters (QFF, Munktell, Sweden).

2.2. Thermal-Optical Carbon Analysis and Time-Resolved Ultra-High-Resolution Mass Spectrometry

2.2.1. Thermal-Optical Carbon Analyzer (TOCA). A DRI Model 2015 Series 1 multiwavelength thermal optical carbon analyzer (TOCA, Aerosol d.o.o.) was implemented. The instrument was conditioned and calibrated according to the manufacturer's guidelines, maintaining a system overpressure of ∼0.5 bar (∼50 kPa) and a total flow rate of 180 to 190 mL/min.

A circular punch aliquot (8 mm diameter, 0.5 cm^2) of the sample is taken for conventional PM analysis. The TOCA oven was heated stepwise following a specific temperature program. The thermal analysis protocol used was IMPROVE_A, which defines 140, 280, 480, and 580 °C as temperature plateaus for the fractions OC1−OC4 in nitrogen (N_2) atmosphere and 580, 740, and 840 °C for EC1−EC3 in a 98 v-% He/N_2 /2 v-% oxygen (O_2) atmosphere. Hereby, OC1 (140 °C) and OC2 (280 °C) can be considered thermodesorption phase, primarily emitting intact molecules, whereas the elevated temperature of

https://doi.org/10.1021/acsmeasuresciau.5c00170
ACS Meas. Sci. Au XXXX, XXX, XXX−XXX

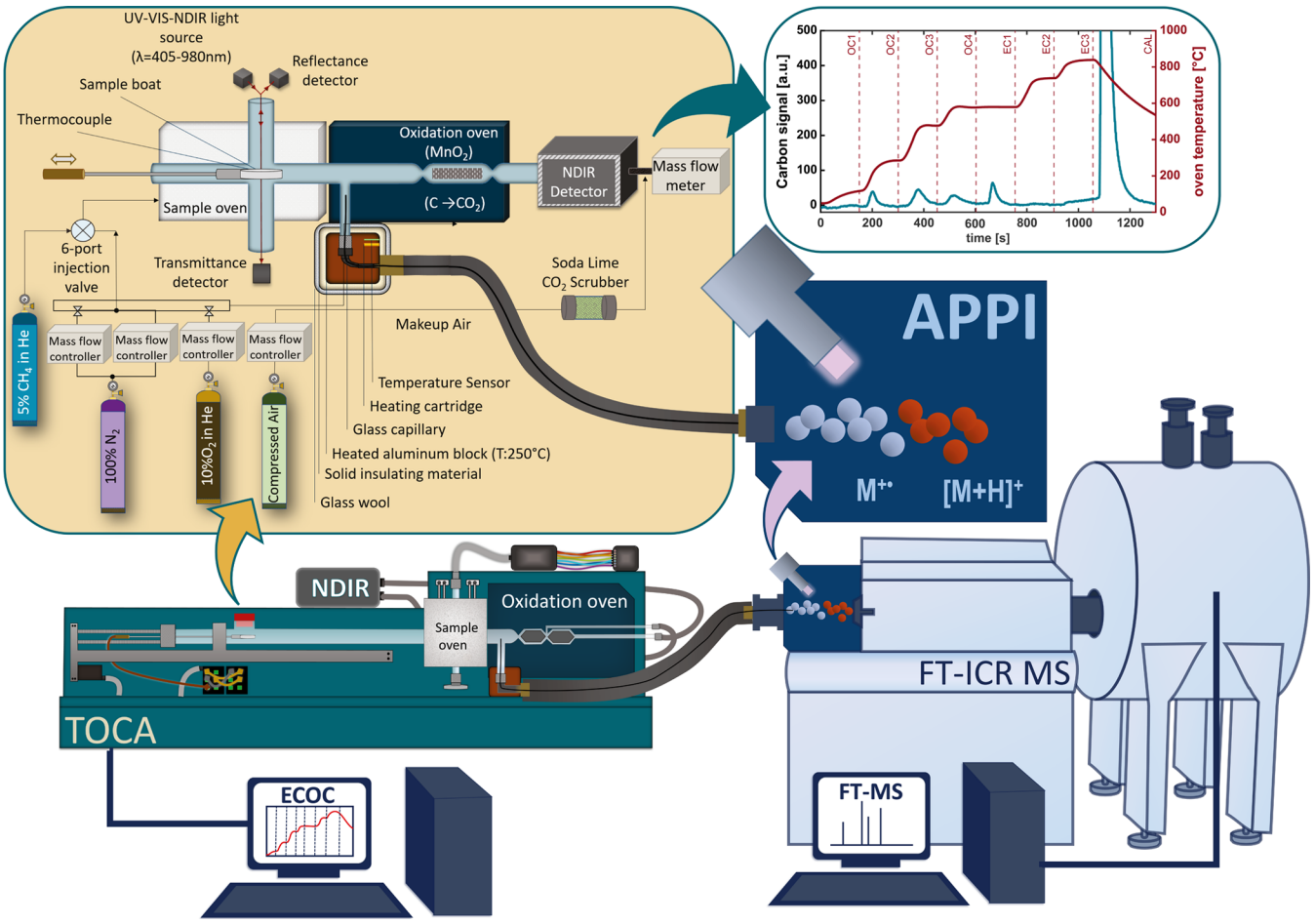

Figure 1. Schematic representation (not to scale) of the hyphenation between the thermal optical carbon analyzer (TOCA) at the bottom left and ultra-high-resolution mass spectrometry (FT-ICR-MS) at the bottom right, including a close-up of the modifications on the quartz cross of the TOCA hyphenation unit. The two platforms are connected via a heated transfer line, which subjects an aliquot of the thermally released compound mixture to the atmospheric pressure photoionization (APPI) source of the mass spectrometer. Photographic illustrations are given in the supporting material (Figure S1).

OC3 (480 °C) and OC4 (580 °C) will induce strong pyrolysis and thermal degradation. The compounds released during the process pass through an oxygenator containing manganese oxide at 900 °C, where they are oxidized and converted into carbon dioxide (CO_2), which is subsequently quantified by a nondispersive infrared sensor (NDIR). At the end of each experiment, the signal is automatically calibrated using 1 mL of 5 v-% methane in helium. During the run, the next temperature step does not commence until the NDIR signal has stabilized or returned to baseline. The duration of each fraction is constrained between a minimum of 150 s and a maximum of 580 s. As a result, the duration of each temperature step varies depending on the amount and release profile of the carbon present.

The optical component of the TOCA includes a UV−vis light source with seven modulated diode lasers, among which the 635 nm wavelength is used for the correction of pyrolytic OC (based on reflectance), along with two detectors, one for measuring reflectance and one for transmission. This optical measurement is required to distinguish between actual elemental carbon and organic carbon pyrolyzed during heating (charring effect). Additionally, blank measurements are taken between samples to monitor and prevent carry-over and memory effects in the MS analysis.

In order to chemically elucidate the evolved gas mixture from OC fractions emitted by the TOCA, a hyphenation to detection via online ultra-high-resolution mass spectrometry (Fourier transform ion cyclotron resonance (FT-ICR) MS, Bruker Daltonics Apex Qe series II, Germany) has been realized. For this purpose, the original quartz cross was modified with an extension of a small, heated quartz side arm between the sample oven and oxygenator.[22] A deactivated fused silica capillary (inner diameter: 320 μm, length: 4 m) is routed from there to the hyphenation unit and subsequently to the transfer line, with the entire coupling heated to 250 °C to prevent recondensation. The overpressure (~0.5 bar) at the TOCA side allows for efficient sampling of the evolved gas mixture into the heated transfer capillary and into the atmospheric pressure (1 atm) ionization source. Considering capillary length and diameter, a split of approximately 100:1 between NDIR and MS analysis can be assumed (restrictor approach, estimate via Hagen−Poiseuille equation).[17] This sampling of an aliquot of the evolved gas mixture is performed before the catalytic oxidation step to carbon dioxide in the TOCA scheme.

For ionization, a modified GC-APCI II ion source (Bruker Daltonics, Germany) was used. The source was modified to allow for atmospheric pressure photoionization (APPI) by

https://doi.org/10.1021/acsmeasuresciau.5c00170
ACS Meas. Sci. Au XXXX, XXX, XXX−XXX

removing the atmospheric pressure chemical ionization corona needle and installing a self-built krypton microwave-induced discharge lamp (10.0/10.6 eV) module tilted from the upper inlet.[15] The instrumental setup is illustrated in Figure 1.

2.2.2. Ultra-High-Resolution Mass Spectrometry: FT-ICR-MS. The time-resolved thermal aerosol analysis by the TOCA IMPROVE_A protocol results in different heating steps (OC1: 140 °C, OC2: 280 °C, OC3: 480 °C, OC4: 580 °C). The chemical profile of the released and sampled mixture is recorded using a commercial 7 T FT-ICR-MS (Apex Qe series II, Bruker Daltonics, Billerica, MA/Bruker Daltonics GmbH, Bremen, Germany) in positive ion mode. The mass spectra recording is continuously performed with a rate of 0.26 to 0.91 Hz, depending on the resolving power setting. This spectral recording was started prior to the TOCA run to collect data on pre-OC and potential high volatile compounds emitted after inserting the sample at room temperature. The procedure for recording evolved gas analysis FT-ICR-MS data was similar to that of Rüger et al.[10] External mass calibration was performed prior to the measurements using known petroleum homologues alkylation-series (CH_2) of a primary ship diesel emission (MGO). This procedure presets the mass analysis to an accuracy generally below 1 ppm, covering a wide mass range of m/z 100−600.

To evaluate the mass spectrometric performance, data acquisition was conducted at variable transient lengths, resulting in different data acquisition sizes (4M: 0.26 Hz, 2M: 0.59 Hz and 1M: 0.91 Hz), proportional to the resolving power and inversely scaling the spectral acquisition rate. This evaluation is described in detail at the beginning of the Results and Discussion section. After evaluation, the optimized conditions have been set to 4M data points, resulting in a resolving power of approximately 260,000 at m/z 400. This setting was used for all other subsequent FT-ICR-MS experiments.

2.3. Data Analysis and Spectral Interpretation

Data analysis was performed via different approaches, i.e., average sums of the entire release pattern, summed intervals of the TOCA fractions (OC1−4, EC1−3), and scan-by-scan full-time-resolved analysis.

For all approaches, initial data processing of the time-resolved high-resolution mass spectra was conducted using Bruker Data Analysis 5.0 SR1. Herein, peak-picking (absolute intensity threshold: 600,000 counts), baseline correction, and internal mass calibration were performed. The latter is done with manually chosen confident assignments and corresponding homologue rows (CH_2, CHO). Mass lists for subsequent chemical annotation are exported by a custom Microsoft Visual Basic (VB) script.[18]

Further processing is performed using a custom-developed tool named CERES, which is based on in-house MATLAB scripting (R2023b).[19] This procedure automatically performs scan-by-scan internal recalibration as well as sum formula attribution. Elemental composition boundaries are adapted based on the specific sample characteristics but generally cover $C_{6-100}H_{6-200}N_{0-2}O_{0-4}S_{0-1}$, H/C 0−3, double bond equivalents (DBE) 0−40 with a sum formula error of less than 1 ppm. The formulas used for calculation of molecular properties are summarized in Section S1 of the supporting material.

3. RESULTS AND DISCUSSION

3.1. Hyphenation and General Mass Spectrometric Response

This section discusses the analytical response of a TOCA hyphenated to APPI-FT-ICR-MS. APPI efficiently ionizes nonpolar and weakly polar compounds with a high sensitivity for aromatic hydrocarbons (AHs) and polycyclic aromatic hydrocarbons (PAHs), which are key markers in aerosol analysis. These compounds reveal emission sources and atmospheric aging, with phenolics indicating biomass burning.[20] Compared to electrospray ionization (ESI) or atmospheric pressure chemical ionization (APCI), APPI has lower matrix effects,[21] and minimal chemical noise, as most solvents and background gases remain nonionized.[22]

Blank measurements confirmed the absence of background signals (Figure S2). TOCA fractions showed no detectable organic or elemental carbon, verifying the cleanliness of prebaked quartz filters. The total ion count (TIC) baseline remained stable, with only instrument-specific frequency noise observed in the spectra. Unlike spray-based techniques like ESI, which often ionize solvent impurities, APPI-FT-ICR-MS exhibited minimal background interference. The frequency noise, characteristic of FT-ICR-MS systems and attributable to ambient radio frequencies or electronic sources, is consistent and readily subtracted during processing, ensuring analytical accuracy.

3.1.1. Acquisition Rate and Resolving Power. For confident molecular attribution, high resolving power and mass accuracy are essential. In time-resolved analysis, the spectral acquisition rate must match the separation speed to preserve temporal characteristics and the emission features. Optimization and evaluation of the acquisition rate are discussed in the following. For this purpose, a representative primary ship diesel sample, known for a complex and broad chemical emission profile was chosen (HS-HFO 2.4 w-% S 60 kW) and three different acquisition parameters are set: 3.83 s scan duration (0.26 Hz repetition rate, $4M/2^{22}$ data points), 1.57 s (0.59 Hz, $2M/2^{21}$) and 1.09 s (0.91 Hz, $1M/2^{20}$). The scan duration in FT-ICR-MS is additionally determined by ion storage and accumulation events, transmission times, data transfer and saving, as well as a millisecond-overhead buffer. Given a stable transient signal, MS resolving power scales linearly with scan time in FT-ICR-MS, whereas an improvement in mass accuracy is often basically a result of a) resolving formerly merged signals, or b) a better definition of the peak apex by adding data points.

Figure 2 summarizes the main results of this parametric investigation. Expectably, the response of the TOCA analyzer, to which approximately 99 v-% of the evolved material is subjected, is not affected across the mass spectrometry parameter set points, indicating good reproducibility of the system. The output data structure of the carbon analysis reports with a 1 Hz time resolution, enabling precise temperature-resolved tracking of the emission profile; thus, only the fastest tested setting of 1M data points, equaling approximately 1 Hz, is directly comparable. Nonetheless, Figure 2a, visualizing the summed mass spectrometric abundance of all detected signals (total ion count, TIC), comes to another conclusion. The emission profile, most dominantly for this sample occurring at organic carbon fraction two (OC2), can be well-described with all three acquisition speeds. The slowest, but mass spectrometrically most powerful

https://doi.org/10.1021/acsmeasuresciau.5c00170
ACS Meas. Sci. Au XXXX, XXX, XXX−XXX

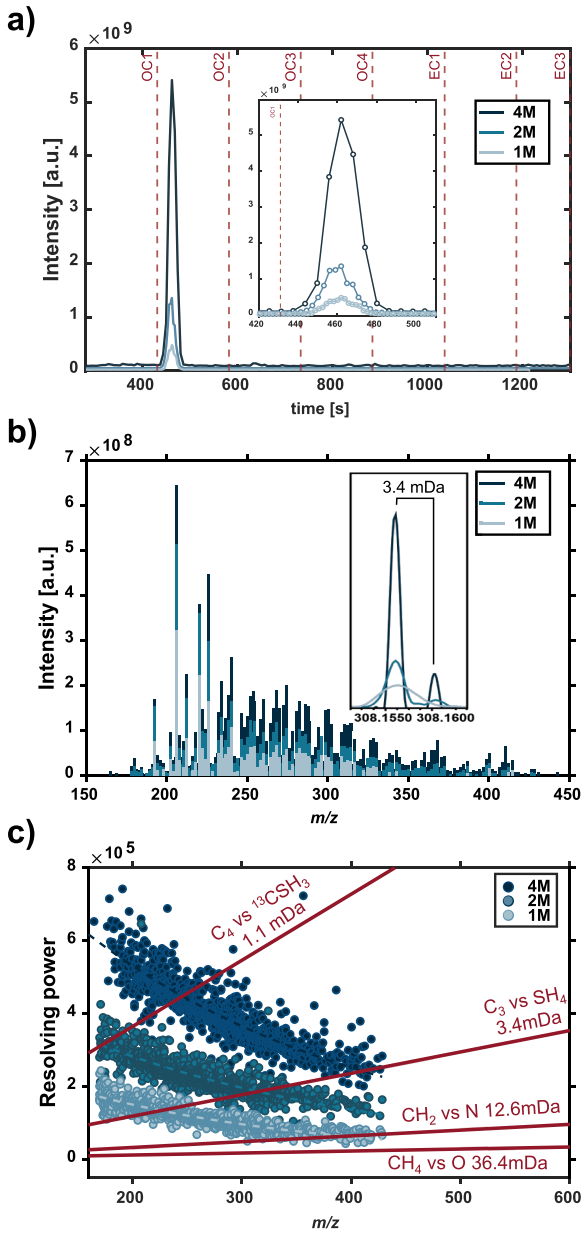

Figure 2. HS-HFO 2.4%S 60 kW engine load analyzed by positive-ion APPI-FT-ICR-MS. (a) Total Ion count (TIC) for 4M, 2M, and 1M measurements. (b) Overlaid mass spectra for 4M, 2M, and 1M with a close-up of a 3.4 mDa mass split (C_3 vs SH_4). (c) m/z versus resolving power scatter plot and critical mass splits in red.

recording of 4M data points still results in a minimum of eight data points describing the rapid evaporation event. A closer examination of the OC2 fraction indicates that increasing the number of data points by using shorter transients (up to over 30) does not significantly improve the TIC description.

The effect of transient length on resolving power (R) is further illustrated in the distribution of resolving power across the m/z range (m/z 150−600), shown in Figure 2c. The expected strong decline in resolving power to higher masses is evident in all measurements and follows the theoretical inverse proportionality of R versus m/z. At the shortest transient length (1M), resolving power is lowest (~70k @ m/z 400), allowing differentiation only for larger mass splits such as 12.6 mDa (CH_2 vs N) and 36.4 mDa (CH_4 vs O). If solely oxygenated species should be differentiated from non-oxygenated compounds at lower m/z, as of high importance in studying the oxygenation-state of aged aerosol emissions, this set point with the highest spectral acquisition rate may be used, improving scan statistics and description of rapid emission profiles. However, the reduced spectral resolution results in extensive peak overlap for multiple other close mass splits, complicating molecular identification, particularly for sulfur-containing compounds (see inset in Figure 2b). Increasing the transient length to 2M improves resolving power by 2-fold (~140k @ m/z 400), enabling the differentiation of more challenging mass differences, such as the 3.4 mDa (C_3 vs SH_4).[23] However, at this data acquisition setting, spectral overlap still occurs, 2M provides moderate spectral precision, but sulfur speciation remains challenging beyond m/z ~320. When using the longest transient length (4M), the resolving power (~260k @ m/z 400) is sufficient to confidently differentiate critical mass splits across the full m/z range observed for the evolved gas analysis in TOCA coupling. At smaller m/z (m/z <300), separations of 1.1 mDa (C_4 vs $^{13}CSH_3$) can be resolved, particularly of importance for spectra with a strong abundance of sulfur-containing compounds, such as in ship emissions from heavy fuel oil combustion.[24,25] This is particularly useful since APPI generates both protonated and radical cations, which differ by this exact mass difference.[26] Sulfur-containing PAHs (S-PAHs), such as thiophenes and benzothiophene moieties, are of current interest in the discussion of compliant shipping fuels and emission abatement technologies, such as scrubber systems, and their environmental and toxicological relevance.[27,28] The enhanced resolving power (4-fold higher compared to 1M) at 4M mitigates the spectral overlap, enabling precise molecular differentiation and improving the reliability of chemical assignments in complex mixtures. At around 300 m/z, this split becomes critical, where 4M resolves it perfectly, 2M begins to struggle, and at 1M shows no discernible split (see 3.4 mDa mass split (C_3 vs SH_4) inset in Figure 2b).

Additionally, reproducibility was evaluated using MGO by analyzing carbon responses from TOCA and APPI-FT-ICR-MS, including emission profiles, mass spectrometric correlation, and compound distribution. TOCA repeatability was assessed via OC/EC fraction comparisons. Consistent thermal desorption patterns were observed, with EC2 contributing most, followed by OC3 and EC1, OC1 showed no response; OC2 and OC3 were nearly equal, and OC4 was minimal (Figures S3, S4). Stable emission profiles across three sample punches confirm the IMPROVE_A protocol's consistency (SD_{OC} = 0.17 μg, SD_{EC} = 3.96 μg, SD—standard deviation) (Figure S3a). EC consistently dominated the emissions (70.14, 72.99, and 65.15 μg), while OC remained lower (27.41, 27.24, and 27.06 μg). The EC/OC ratios (2.56, 2.68, 2.41) and reproducibility ($SD_{EC/OC}$ = 0.14) align with manufacturer specifications and literature benchmarks.[29,30]

In the mass spectra, OC2 also exhibited the highest TIC. TIC profiles were comparable in intensity, timing, and width, indicating consistent sampling and analysis of the evaporated gas mixture (Figure S3b). Reproducibility was confirmed by high congruence coefficients (>0.981; Table S2), reflecting strong spectral similarity across replicates. This consistency is further supported by similar compound class distributions (CH, CHO, CHO_2) and stable chemical profiles (Figure S3c). Regarding chemical composition, from 532 shared compounds, unique detections per sample were below 8%, contributing less than 5% of total intensity. In contrast, shared compounds

https://doi.org/10.1021/acsmeasuresciau.5c00170
ACS Meas. Sci. Au XXXX, XXX, XXX−XXX

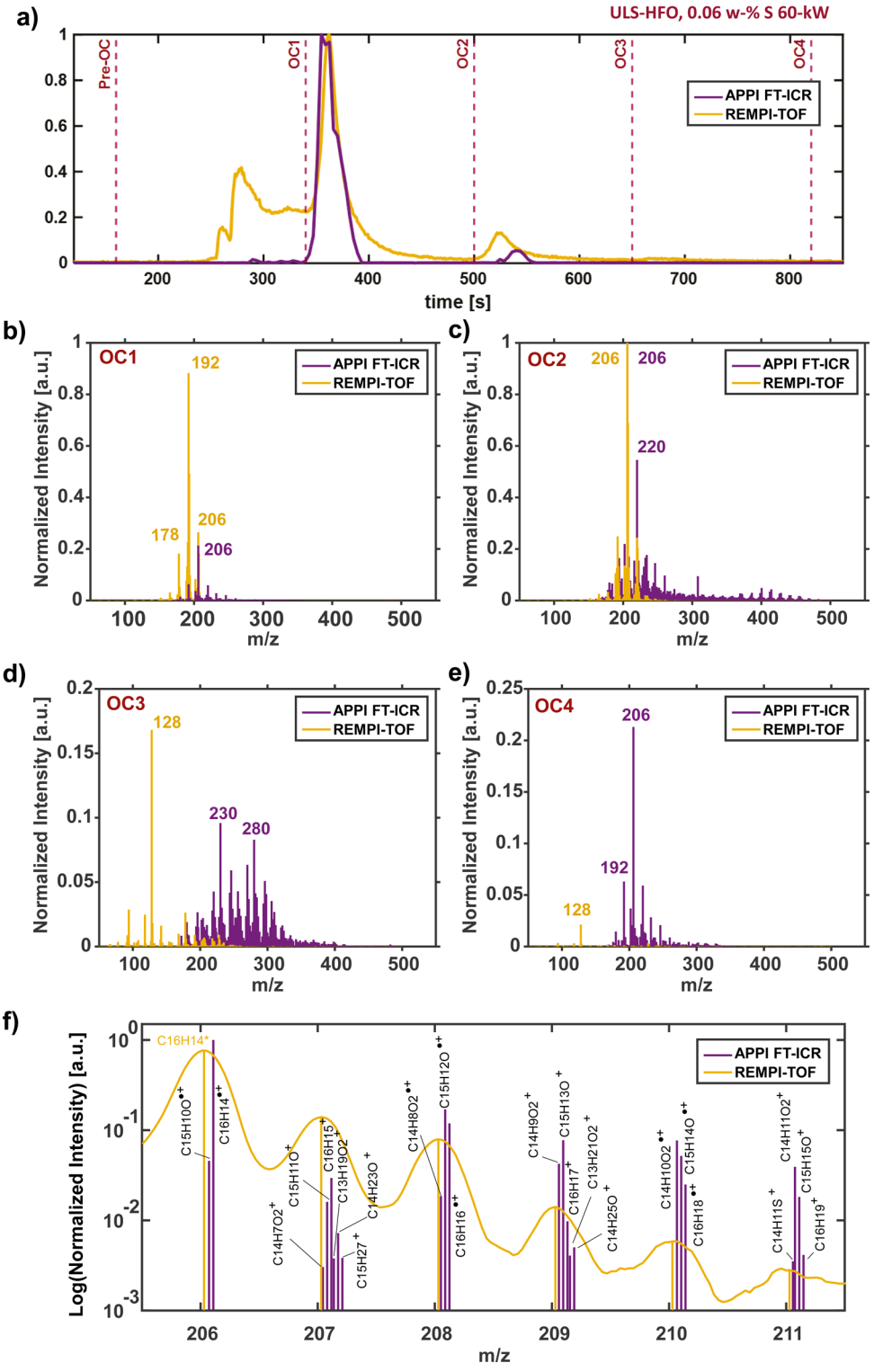

Figure 3. Comparison of the results from a TOCA measurement of a primary ship diesel emission (ULS-HFO, 0.06 w-% S 60 kW) with high-resolution APPI-FT-ICR-MS (violet) and unit mass resolution REMPI-ToF-MS evolved gas analysis (yellow). (a) Total ion count (TIC), with averaged mass spectra for the individual IMPROVE_A protocol fractions: (b) OC1, (c) OC2, (d) OC3, and (e) OC4, normalized to the highest signal (m/z 206, $C_{16}H_{14}^{+\bullet}$). (f) Zoomed-in view of the OC2 fraction in the nominal mass range (m/z 205−212) normalized with a log scale on the y-axis. The FT-ICR data reveal various oxygenated compound classes, including CH- and CHS-constituents. The 3.4 mDa split (C3 vs SH_4) is resolved. Isotopes have been removed from the APPI-FT-ICR-MS data for clarity following the chemical annotation.

represented over 95% of the signal intensity (Figure S3d). These results demonstrate high reproducibility in both spectral and compositional data, comparable or superior to other high-resolution evolved gas analysis methods like DIP or ASAP.[31,32]

We could show that in hyphenated thermal analysis, balancing acquisition speed with spectral resolution is critical, particularly considering the mass spectrometric specifics of FT devices, such as FT-ICR-MS and Orbitrap MS. Longer

https://doi.org/10.1021/acsmeasuresciau.5c00170
ACS Meas. Sci. Au XXXX, XXX, XXX−XXX

transients improve frequency resolution, signal-to-noise ratio, peak accuracy, and ion separation, with 4M transients providing optimal performance, with a trade-off in temporal resolution. Consequently, in the following, this transient length was chosen for all analyses to ensure high mass accuracy and resolving power. The chosen acquisition parameters allowed for real-time detection of the evolving species from the TOCA, preserving temporal data integrity and ensuring precise analyte characterization (Tables S2, S3).

3.1.2. FT-ICR-MS versus ToF-MS Response. The molecular description of the evolved gas mixture in TOCA has been previously reported primarily using resonance-enhanced multiphoton ionization time-of-flight mass spectrometry (REMPI-ToF-MS). This concept has been extensively used by our group for the detection and monitoring of aromatic species in a wide range of combustion processes.[4,12] Here, we compare the instrumental responses and discuss the analytical differences between the REMPI-ToF-MS setup operated at 266 nm, and the proposed APPI-FT-ICR-MS methodology.[33] For this purpose, four samples were analyzed on both complementary platforms. Both techniques feature soft ionization, providing access to molecular information. Another work utilizes mass spectrometry to access elemental information, such as nitrogen and sulfur content.[34] However, this work commonly features hard electron impact ionization, which is not comparable to the soft nature of APPI presented in this context.

Investigation of the TIC obtained from both mass spectrometric technologies reveals striking differences (Figures 3a, S5). Although the TIC suggests broader coverage, REMPI-ToF-MS primarily captures emissions in the lower m/z range across the different OC fractions. Solely for the OC2 fraction, both techniques exhibit similar ion signal and emission profile. However, the averaged mass spectra for the individual fractions reveal complex mass spectrometric patterns for OC1−4 for both systems. The similarity for the OC2 fraction indicates that both platforms are detecting a similar range of compounds. This argument is underpinned by the respective mass spectra (Figure 3c), revealing a high similarity for the most dominant species between m/z 180−220 for both systems. However, APPI enables broader coverage up to m/z 450 with a complex pattern dominated by an overlapping alkylation pattern (CH_2 homologue series).

Generally, the detection of low-mass compounds by FT-ICR-MS is largely limited due to multiple physical and instrumental constraints, such as time-of-flight effects in the ICR cell injection (mass range coverage), magnetic mirror effects, or excite/detect compatibility.[35,36] Consequently, most FT-ICR-MS systems with external ion supply have a lower m/z cutoff of approximately 100−150.[10] In the presented case, the specific platform was tuned for efficient coverage in a mass region of m/z 150−1000; as mathematical possibilities of sum formulas drastically scale with mass, commonly higher m/z require ultrahigh mass spectrometric resolution. Lower-mass species are better covered by W-mode HR-ToF-MS systems or are even addressed by mass analyzers with unit mass resolution, such as quadrupole devices or the REMPI-ToF-MS employed as a comparative mass spectrometer in this study. The absence of TIC peaks for the OC1, OC3, and OC4 fractions for the FT-ICR-MS can be attributed to the low molecular weight cutoff. The desorbed compounds in OC1 are low-mass-weight, high-volatile species, as detected with the REMPI-ToF-MS, and only a particular overlap starting at m/z 180 is efficiently covered by the FT-MS device (Figure 3b). In OC3 and OC4, the temperature has risen to high values, inducing strong pyrolysis of the carbonaceous aerosol compounds. This pyrolysis tends to predominantly form smaller thermal fragments, such as seen in Figure 3d/e for the REMPI-ToF-MS analyzer, featuring negligible m/z transmission and detection bias via ionization selectivity. However, the APPI-FT-ICR-MS is able to sensitively cover remnants of larger m/z compounds. The same observation has been made in the coupling of thermal gravimetry to APPI-FT-ICR-MS for a wide variety of petroleum samples.[37] The overpressure generated by the TOCA effectively promotes the transfer of evolved gases into the APPI source, yielding an instrumental response that remains broadly consistent with that of the vacuum ionization ToF-MS, taking into consideration natural and instrumental differences in mass range coverage.

A comparative zoom-in to m/z 206−211 of the summed mass spectra of the OC2 fraction allows addressing the mass spectrometric performance, with respect to the resolving power (Figure 3f). The FT-ICR-MS is able to fully resolve all mass signals in the given segment, and sum formulas are attributed with errors generally below 1 ppm. Isotopic peaks, used in the automated data processing for increasing the annotation confidence, are removed from this figure to improve the visualization. The REMPI-ToF-MS with unit mass resolution is not able to resolve any of the given mass splits at the nominal mass level. However, chemical information is commonly retrieved taking into consideration the enhanced selectivity of REMPI toward aromatic compounds, particularly PAHs. Using this strategy, m/z 206, likely $C_{16}H_{14}^{+\bullet}$, is attributed to a C2-alkylated three-ring PAH. Based on differences in ionization cross section and knowledge of sample characteristics, e.g., combustion source and conditions, the presence of a C2-phenanthrene can be speculated. The comparison of signal-to-noise ratios (S/N) for this target shows that APPI-FT-ICR-MS exhibits a substantially higher S/N (>12,000) than REMPI-ToF-MS (1,785.8), reflecting the superior ion accumulation and long transient detection of APPI-FT-ICR-MS, which enhances signal intensity despite the preferential ionization of aromatic species in REMPI. In contrast, APPI-FT-ICR-MS does not give direct structural annotation but resolves underlying nominal mass splits and indirect structural data via sum formula information. For m/z 206, APPI-FT-ICR-MS also detects $C_{16}H_{14}^{+\bullet}$, tentatively attributed to isomers of C2-alyklated three-ring PAHs, as the most abundant signal at this nominal mass. However, with a lower abundance of approximately 1 order of magnitude, an oxygenated compound ($C_{15}H_{10}O^{+\bullet}$, 36.4 mDa mass split, CH_4 versus O) can be clearly resolved, detected, and attributed. The DBE of this compound is 11, and molecular libraries suggest a poly-aromatic structure, featuring an aldehyde, furan or alcohol functionality. This compound is likely to be ionized in REMPI,[38] but its signal is expected to be very low under typical wavelengths (248−266 nm), making detection challenging given the limited resolving power.

Although APPI and REMPI are both photoionization techniques, the chemical space coverage for APPI is drastically higher, and ionization of a broader range of molecular classes and chemical functionalities is achieved, whereas REMPI is particularly selective for AHs and PAHs. As FT-ICR-MS handles compositional complexity through mass spectrometric resolution, this APPI characteristic is beneficial, allowing for the ionization and annotation of additional chemical classes,

https://doi.org/10.1021/acsmeasuresciau.5c00170
ACS Meas. Sci. Au XXXX, XXX, XXX−XXX

such as oxygenated species or sulfur-containing compounds. Although such compounds can be ionized by REMPI when heteroatoms are ring-bound, APPI generally provides higher efficiency, particularly for low-DBE and less aromatic compounds. Compounds of high relevance in aerosol science but likely missed by ionization cross-section limitations in vacuum REMPI. Nonetheless, APPI not only generates radical cations (odd-electron configuration $[M]^{+\bullet}$), but to a certain extent also protonated ions (even-electron configuration, $[M + H]^+$). This characteristic adds complexity to the spectral response and potentially diverts the ion signal of one analyte into two mass channels. Ultimately, it also highlights the ultra-high resolving power, as ionization of sulfur-containing species (see Figure 3f, nominal mass 211) results in a C_3/SH_4 split (3.4 mDa), a level of detail unresolved by TOF-based instruments.

The proven level of detail in the molecular description of carbonaceous aerosols is likely to be highly valuable for in-depth chemical description. Consequently, the presented methodology is applied to various aerosol types, and the fractionated information from the TOCA-FT-MS analysis is discussed.

3.2. Application toward Characterization of Carbonaceous Aerosols

3.2.1. Ship Emissions. Primary combustion emissions from ship diesel engines serve as a common case for anthropogenic carbonaceous aerosols. To reduce their environmental and health impact, Sulfur Emission Control Areas (SECAs) limit the maximum sulfur content in fuels, leading to the adoption of low-sulfur fuels and abatement technologies such as scrubbers. The combustion of heavy fuel oils (HFOs) and MGO produces complex carbonaceous aerosols, with composition strongly influenced by fuel type, sulfur content, and engine load. To capture this variability, our data set includes high-sulfur HFO, ultra-low-sulfur HFO, and MGO, with some fuels analyzed at two engine loads.

3.2.2. Residential Wood Combustion. Residential wood combustion (RWC) in northeastern and central Europe poses serious health and environmental risks due to particulate matter, high PAH levels and oxygenated compounds.[39−41] These emissions differ from shipping fuels by being sulfur-poor but relatively nitrogen- and oxygen-rich, producing more polar organic compounds. RWC therefore provides a complementary test case to evaluate our hyphenated approach for biomass burning aerosols.

3.2.3. Ambient Aerosols. Ambient urban aerosols are chemically complex due to contributions from diverse emission sources and atmospheric aging processes. To assess the applicability of our methodology under real-world conditions, we analyzed two ambient aerosol samples, one from autumn, and one from spring from a Beijing campaign. This data set, studied by Shen et al. (2016, 2018), highlights substantial seasonal variability, with contributions from biomass burning, coal combustion, and secondary aerosol formation.[42,43]

3.2.4. Thermal-Optical Carbon Analysis (TOCA) Response and Molecular Functionality across Sample Types. Thermal−optical carbon analysis (TOCA) provides an initial overview of the bulk carbonaceous composition of the investigated samples, complementing molecular-level insights obtained from high-resolution mass spectrometry. While the carbon characteristics of the emitted particulate matter have been described in detail elsewhere;[44,45] a brief summary is provided here to place the evolved gas profiles in context with the molecular signatures.

The carbon analysis and mass spectrometric evolved gas analysis for ship engine emissions exhibited a strong contribution from the OC2 fraction across all fuels (Figure S6). The limited mass range coverage, particularly for lower-mass compounds, accounts for the absence of mass spectrometric responses, despite measurable carbon release at OC4. In particular, ULS-HFO exhibits an additional stronger signal for the OC3 fraction, significantly more pronounced compared to HS-HFO and MGO, consistent with its formulation, as a distillate−cycle oil blend enriched in heavier aromatics compliant with SECA regulations.[27,28] Due to the substantial amounts of aromatics, such blended fuels are more likely to ionize efficiently within the m/z-range of our mass spectrometer, explaining the pronounced OC3 signal observed.

The molecular fingerprints of these emissions across the m/z 180−500 range displayed a characteristic m/z 14 spacing, resulting from a dominant alkylation pattern of core structural motives, commonly found in *Petroleomics*. Such patterns are indicative of unburned fuel, which constitutes a major contributor to marine engine particle-phase emissions. Residual hydrocarbons that undergo incomplete thermal transformation retain the alkylated structures typical of petroleum-derived mixtures, thereby shaping the observed mass spectra. Across all fuel types, CH-class has been found to be the most abundant, followed by the CHO- and CHS-classes, reflecting the hydrocarbon-rich chemistry of marine fuels (Figure S7). HS-HFO combustion produced complex emission profiles, with 706 assigned sum formulas, and with up to 10 signals, with an average of 2.4 sum formulas, per nominal mass. MGO shows comparatively lower emission complexity with fewer sum formulas (682 compounds) and an average of 2 sum formulas per nominal mass. The MGO 60 kW sample, was dominated by CH- and CHO- classes, consistent with previous studies on MGO fuels.[15] Meanwhile, the ULS-HFO yielded the richest chemical diversity (≈950 compounds), including a few nitrogen-containing species (CHN_1O_x, x = 1−2). Sulfur compounds were not detected in any fraction for emissions from the ship diesel engine operated with "clean" distillate fuel MGO, nor in ULS-HFO emissions, consistent with the feed fuel chemistry and the ionization selectivity.

In contrast, RWC displayed a distinctly different TOCA response, characterized by the strongest overall evolved gas signal among all sources. The profile was marked by a prominent EC1 peak (Figure S8a), which, however, was absent in the corresponding mass spectrometric traces, where OC2−OC3 fractions dominated the TIC profile (Figure S8b). The absence of EC1 in the mass spectra is due to the refractory, highly condensed nature of elemental carbon, which resists ionization under APPI conditions. In contrast, typical PAHs formed during the efficient combustion process, such as $C_{16}H_{10}$ (fluoranthene and pyrene), $C_{20}H_{12}$ (benzofluoranthene and benzopyrene), and $C_{22}H_{12}$ (indenopyrene and benzoperylene) are notably prominent (Figure S8c).[46] These combustion-derived PAHs, including toxic or carcinogenic compounds such as benzo(a)pyrene, highlight the potential health risks associated with RWC emissions. The compound class distribution shows a greater contribution from the CH-class, followed by oxygenated species.[47] This is accompanied by an increase in the average number of oxygen atoms in the CHO-class compared to those typically observed in ship emissions, as well as the detection of CHNO compounds. In

https://doi.org/10.1021/acsmeasuresciau.5c00170
ACS Meas. Sci. Au XXXX, XXX, XXX−XXX

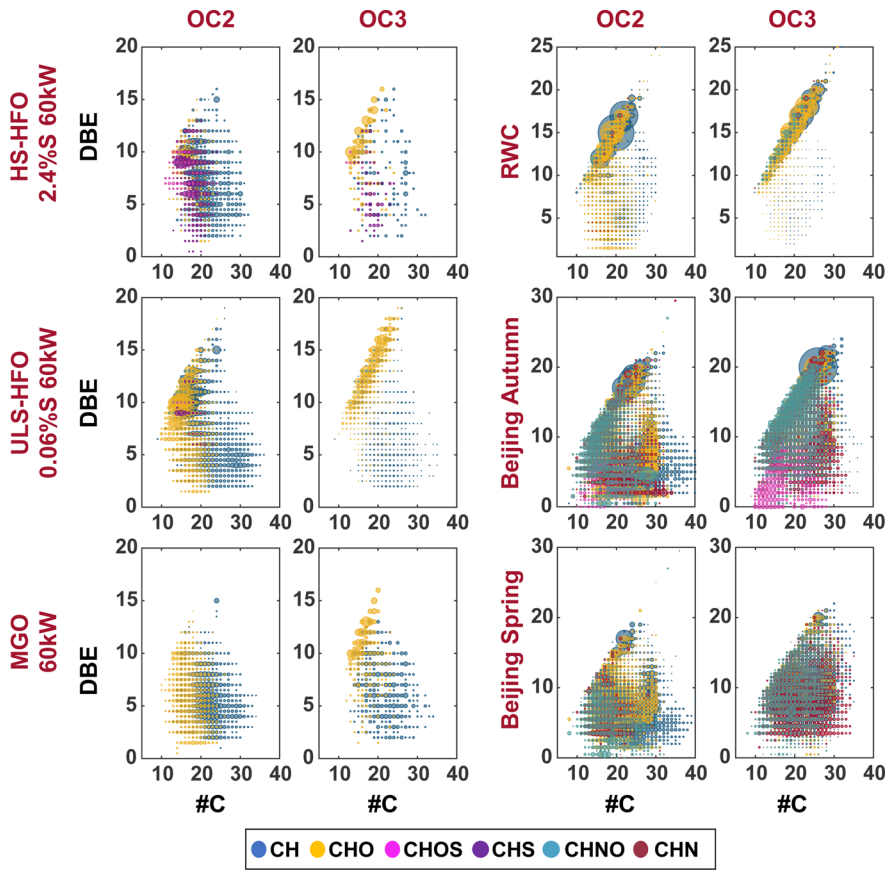

Figure 4. Aromaticity (DBE) versus carbon number (#C) for fractions OC2 and OC3 from HS-HFO 60 kW (left top), ULS-HFO 60 kW (left middle), and marine gas oil (MGO) 60 kW (left bottom). Residential wood combustion (RWC) (Right top), Beijing autumn (Right middle) and Beijing spring (right bottom) ambient samples. Compound classes are represented by color, with relative intensity indicated by dot size. Intensity normalized to each fraction.

total, 1353 distinct compounds were detected, exceeding the number observed for marine engine emissions, reflecting the chemical complexity of biomass combustion. Nitrogen-containing species were detected, with CHN compounds accounting for up to 3.5% and CHNO compounds making up to 12.7% of the total number of compounds detected across the OC fractions, corresponding to 1.8% and 5.5% of total ion intensity, respectively, as shown in Figure S8d.

Consistent with combustion-derived complexity, ambient aerosols from Beijing illustrated yet another distinct TOCA emission profile characterized by a higher proportion of organic carbon (OC) relative to elemental carbon (EC) in both autumn and spring samples. Both samples exhibit OC-dominated profiles (Figure S9a), with OC concentrations reaching 80.5 $\mu g\ m^{-3}$ in autumn, and 51.4 $\mu g\ m^{-3}$ in spring, accompanied by EC maxima of 22.1 $\mu g\ m^{-3}$ and 16.3 $\mu g\ m^{-3}$, respectively. The OC3 and OC4 fractions accounted for the largest share of total OC, reflecting the dominance of thermally stable organic material in the ambient samples. The stronger charring response compared with MGO samples indicates that a larger fraction of the organic matter undergoes carbonization during heating, consistent with the presence of complex, combustion-derived organic compounds.[12,48] The elevated OC/EC ratios (3.6 in autumn, 3.2 in spring) further support the prevalence of organic-rich emissions, with contributions that may include secondary organic aerosol alongside primary combustion sources, such as biomass burning.[49,50] The mass spectrometric response revealed a pronounced signal across the OC1−OC3 fractions, with particularly intense distributions observed in both seasons. From the OC2 fraction onward, a shift toward lower m/z values was detected, suggesting the onset of thermal fragmentation processes (Figure S9b). Notably, highly condensed PAHs demonstrated strong thermal resilience, especially in autumn, where $C_{24}H_{14}$ dominated the OC2 signal, followed by $C_{26}H_{14}$ in OC3 and $C_{28}H_{14}$ in OC4, indicating the presence of large, combustion-derived aromatic structures. Arithmetic means of the parameters calculated from each elemental composition as well as annotation number for the sample types is summarized in Table S4.

3.2.5. Molecular and Aromaticity Characteristics of Carbonaceous Aerosols. For describing aromaticity and chemical trends, carbon number (#C) versus double-bond equivalent (DBE) diagrams are widely used in high-resolution mass spectrometry of complex mixtures. Figure 4 presents the #C versus DBE pattern color-coded according to compound class for selected OC2 and OC3 fractions with strong response (additional OC1 fraction visualized in Figure S10).

In ship emission samples OC1 fractions are dominated by CH-class compounds with low heteroatom content (less than 30%, based on molecular formula assignments), with MGO containing the least at 20% (Figure S10). This fraction primarily consists of desorbed species with a low carbon number (<25 #C) and with low DBE values suggesting primarily one- and two-ring aromatic moieties. In contrast, HS-HFO exhibits values up to DBE 10, including three-ring aromatics, such as alkylated phenanthrenes ($C_{14}H_{10}^{\bullet+}$ + *n*-

https://doi.org/10.1021/acsmeasuresciau.5c00170
ACS Meas. Sci. Au XXXX, XXX, XXX−XXX

CH_2, DBE 10). The ULS-HFO shows a narrow distribution centered at high DBE values, indicating a low chemical diversity for the species evaporable up to 140 °C (OC1) with mostly core structure two-to-three-ring PAHs and low alkylated derivatives thereof.

Regarding OC2, a pronounced shift toward more oxygenated and sulfur-containing compounds is observed. ULS-HFO contains approximately 60% of assigned heteroatom species, dominated by CHO-, CHOS-, and CH-classes, whereas MGO remains lowest at 53% with only the CHO-class (Figure 4). In addition, the chemical space increased with carbon numbers from 10 to 35 and DBE from almost 0 to 20. For instance, HS-HFO exhibits sulfur-containing species clustered at DBE 6 and 9, likely alkylated thiophenes and dibenzothiophenes/naphtho-thiophenes. On the other hand, MGO features a dense distribution with lower DBE values dominated by naphthenic (DBE < 4) to three-ring PAHs (DBE 11), with heavy alkylation. The oxygenated compounds revealed shorter side chains (lower m/z) compared to the respective CH-class analogues. For the HFOs, especially ULS-HFO, a pronounced cluster of signals emerges near the planar aromatic limit, with values up to DBE 15, indicating thermal release/volatilization of four- and five-ring PAHs, at 280 °C. However, also for these fuels, heteroatom-containing species are substantially lower in weight compared to their CH-class counterparts. Despite this aromatic enrichment the signal intensity of heteroatom-containing compounds is far lower than their CH-class counterparts. At 480 °C (OC3), analytical pyrolysis produces thermally stable, high-boiling compounds that approach the planar aromatic limit, suggesting highly condensed molecular structures. These species consist mainly of PAH core structures, with limited alkylation (up to n = 5) and heteroatom-containing derivatives formed by side-chain cleavage during pyrolysis. Within the context of complex petrochemicals, such distribution is commonly described as a single core ("island") molecular architecture, in contrast to the more alkylated, multicore ("archipelago") structures found at lower DBE and higher alkylation (carbon number).[51−53] The strong OC3 response evident in the TIC distribution is thus molecularly explained by abundant CHO- and CH-class species concentrated in this condensed aromatic region, consistent with the feed fuel composition as a blend enriched in high-boiling, highly aromatic constituents. Across ship emission and independent of the fuel type, this planar aromatic limit region is mostly populated by CHO-class compounds, whereas CHS- or CH-class compounds appear at lower DBE and higher carbon numbers. Notably, ship emissions frequently contain large proportions of unburned fuel, increasing the relevance of the fuel chemistry and refinery process.[19,30,54] The last organic carbon fraction (OC4) primarily consists of small, low-molecular-weight compounds, resulting from desorption and extensive thermal cracking, with very low intensities that are hardly detectable by APPI-FT-ICR-MS.

The structural motifs discussed are also applicable to biomass combustion. In this context, the RWC sample reveals a broader DBE-to-carbon number region compared to ship emissions (Figures 4, S11). OC1 fraction is represented by alkylated one- to three-ring PAHs (up to C30), while subsequent fractions are enriched in CHO- and CHNO-classes. The OC3 and OC4 fractions cluster along the planar limit, consistent with island-type motifs (highly aromatic cores), but extend across a wider DBE range, including oxygen- and nitrogen-containing species.

With respect to ambient samples, seasonal variation in aromaticity (DBE) and molecular size (C#) is evident. In autumn, the OC1 fraction is dominated by CHO-class compounds, likely originating from biomass combustion (Figure S12). Characteristic species include terpenoids ($(C_5H_8)_{3-6}$), and O-PAHs, with molecular formulas such as $C_{13}H_8O$ (DBE 10), $C_{15}H_{12}O$ (DBE 10), $C_{14}H_8O_2$ (DBE 11), and homologous compounds differing in the number of $-CH_2-$ units. Both spring and autumn aerosols display broad compound distribution with compounds containing up to 35 carbon atoms, indicating the presence of more aliphatic compounds with longer alkyl chains. In the OC2 fraction, CHN- and CHNO-class compounds become more prominent, appearing as both condensed aromatic and aliphatic structures (Figure 4). This pattern may be linked to secondary organic nitrate formation for CHNO species, while CHN compounds are primarily combustion-derived or potentially formed through condensation reactions between carbonyls and amines, as observed in brown carbon (BrC) formation.[55] Additionally, the detection of hopanes ($C_{27-32}H_{46-52}$)[56,57] in both samples suggests a contribution from fossil fuel combustion. While commonly associated with lubricants in gasoline and diesel engines, these compounds can also derive from coal combustion, which was prevalent in Beijing at the time. The analysis of the autumn OC3 fractions reveals that sulfur-containing species account for approximately 6.7% of the detected compounds, reflecting either thermally fragmented larger molecules from anthropogenic sources, such as industrial or urban emissions, or the presence of organic sulfates, which are likely underestimated.[58,59] In spring, the CHN-rich compounds observed in the OC3 likely originate from thermally refractory nitrogen-containing species that survive the high-temperature program. These include a combination of highly functionalized organic nitrates and nitrate-bearing oligomers formed via nocturnal NO_3 chemistry or photochemical aging of biogenic VOCs, as well as nitro-aromatic residues from biomass burning. Since labile organonitrates would have decomposed at lower temperatures (<480 °C), the CHN signals in the OC3 fraction serve as a marker of persistent organic nitrates and nitro-aromatics, reflecting mixed contributions from biomass burning, agriculture, and secondary organic aerosol formation influenced by NO_x chemistry.[60,61]

Complementary insight into the degree of oxidation and functionalization of aerosol fractions can be gained using Van Krevelen diagrams (H/C vs O/C). In the case of ship emissions, a consistent fraction-resolved trend across fuel types was observed (Figure S13a). The OC1 fractions cluster mostly at high H/C ratio and near-zero O/C values, indicating hydrogen-rich compounds with minimal oxygen content. Meanwhile, OC2 and OC3 cover a broader range; OC2 exhibits a slightly higher H/C ratios than OC3 and intermediate O/C values, consistent with semivolatile oxygenated compounds, while OC3 shifts toward lower H/C and O/C ratios, reflecting more stable, aromatic-rich species, alongside highly oxygenated compounds reaching larger O/C values. OC4, although sparsely populated, lies at even higher O/C ratios, indicative of heavier, highly condensed oxygenated compounds remaining after prior pyrolysis steps. Overall, the intensity-weighted averages (diamonds in Figure S13) show a clear progression toward higher O/C with increasing OC fraction, accompanied by lower H/C values in the pyrolytic fractions (OC3/4) compared with the intact desorption

https://doi.org/10.1021/acsmeasuresciau.5c00170
ACS Meas. Sci. Au XXXX, XXX, XXX−XXX

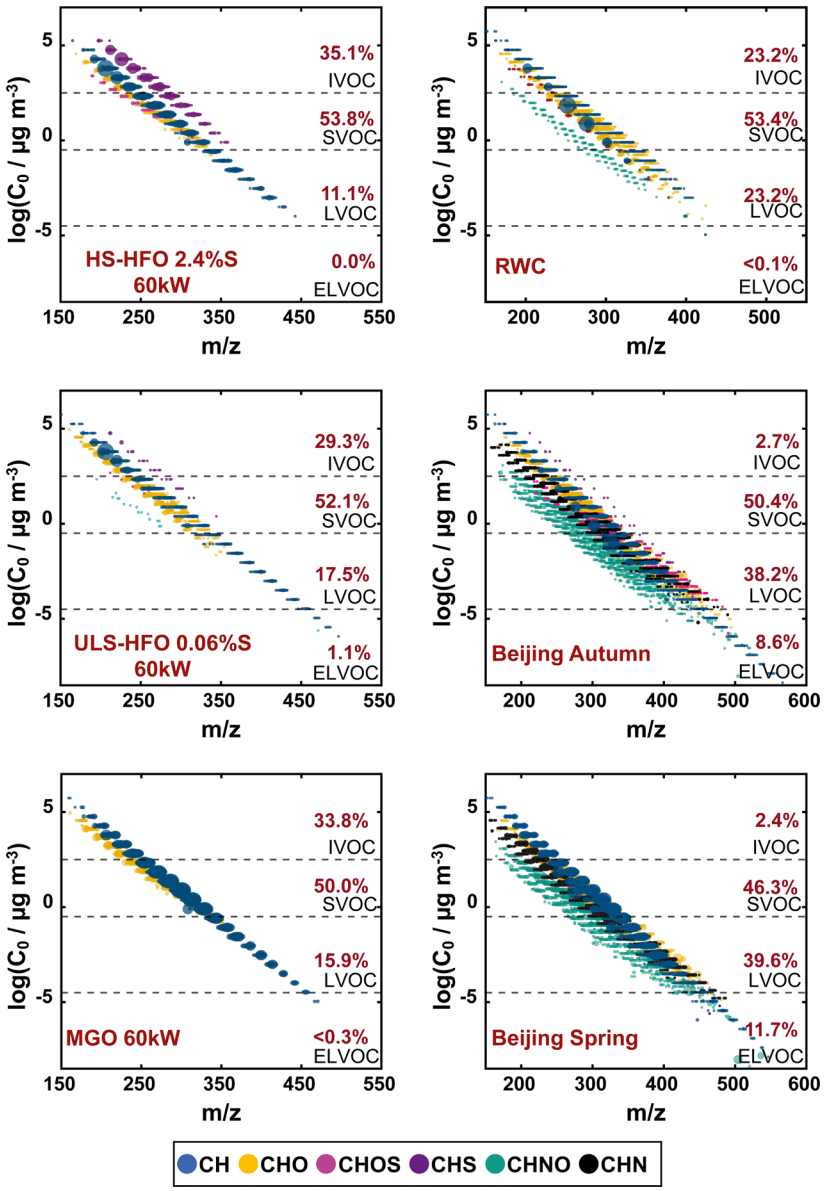

Figure 5. Plot of the calculated saturation mass concentration (C_0) versus m/z ratio is presented, highlighting the organic compounds and their corresponding compound classes. Samples include HS-HFO 2.4%S at 60 kW, ULS-HFO 0.06%S at 60 kW, Marine Gas Oil (MGO) at 60 kW), Residential wood combustion (RWC), and Beijing ambient samples autumn and spring. Compound classes are represented by color, with relative intensity indicated by dot size. Volatility ranges for intermediate-volatile organic compounds (IVOCs), semivolatile organic compounds (SVOCs), low-volatile organic compounds (LVOCs), and extremely low volatile organic compounds (ELVOCs) are indicated by horizontal dotted lines. Sum formula annotations from all OC fractions (OC1−4) are combined in this visualization.

fractions at lower temperatures (OC1/2). Consistent with the #C versus DBE diagram, most OC3 compounds fall within the PAH regime, highlighting their aromatic-rich character.

Compared with the composition of shipping fuel emissions, RWC compounds cluster at lower H/C and high O/C ratios in the Van Krevelen diagram (Figure S13b; Table S4), reflecting heavier, less volatile molecules enriched in oxygenated functional groups, such as alcohols and ketones. Highly unsaturated CHN-class compounds are also prominent, likely N-PAHs such as $C_{21}H_{13}N$, $C_{21}H_{11}N$, and $C_{23}H_{13}N$, which were identified in the RWC sample and are consistent with previous reports on biomass burning.[62] Furthermore, CHNO-class compounds appear at high O/C ratios and display a pronounced aromatic character. These species are considered significant contributors to Brown Carbon (BrC) due to their strong light-absorbing properties.[63,64]

The Van Krevelen diagrams of the ambient samples do not display strong seasonal contrasts, but some differences are evident. During the autumn sampling period, OC1 and OC2 were more prominent, indicating semivolatile compounds with relatively low oxygenation, likely associated with primary emissions such as fossil fuel combustion or biogenic sources (Figure S13c). The spring sample, however, showed a higher contribution from OC3, consistent with a more aged and oxidized aerosol composition.

3.2.6. Volatility and Mass Distribution of Organic Aerosols. The presence of heteroatoms strongly influences the volatility of organic compounds, as nitrogen- or oxygen-containing species generally desorb at higher temperatures

https://doi.org/10.1021/acsmeasuresciau.5c00170
ACS Meas. Sci. Au XXXX, XXX, XXX−XXX

than pure hydrocarbons. Oxidation further increases polarity, reducing vapor pressure, and shifting oxidized species from desorption to pyrolysis during thermal analysis. Although saturation mass concentration can be used to classify organic compounds by volatility, its application in most evolved gas analysis (EGA) MS methods is limited because electron ionization (EI) often causes extensive fragmentation, which hinders the detection of molecular ions. To address this, our approach employs low-fragmentation ionization, which simplifies spectra and enables more reliable structural characterization. High resolving power allows discrimination of isobaric features and accurate elemental composition assignment, resolving mass differences below 10 mDa commonly found in complex aerosol samples.

Although saturation mass concentration (C_0) is generally not employed in fuel emissions analysis, we introduced it here to facilitate comparison with biomass burning and ambient aerosols. The volatility (C_0) was calculated using the parameterization of Li et al.[65] Input parameters including compound classes and their respective n^0_C and b values are summarized in Table S5. In engine combustion samples (Figure 5, left panels), semivolatile organic compounds (SVOCs) account for the largest share, about 50% of the total abundance, followed by intermediate-volatile organic compounds (IVOCs) (~30%), and low-volatile organic compounds (LVOCs) (<20%). For HS-HFO, the average log(C_0) value is 1.87, consistent with previous IVOCs studies,[66] indicating substantial contribution from high-boiling-point compounds, including heterocyclics, to low-volatility organic emissions. Among engine samples, ULS-HFO exhibits the highest average log(C_0) with 2.06, which aligns with evidence suggesting that the use of ultra-low-sulfur oil is associated with higher IVOC emissions.[66] Nitrogen-containing compounds remain within the SVOC range, while low combustion efficiency promotes IVOC emissions.[67] The lowest average log (C_0) with 1.22 is found in MGO. Although calculated across all fractions, the predominance of OC2 suggests that most of the species are derived from the desorption process.

In contrast to engine emissions, fresh RWC PM contains higher proportions of SVOCs resulting from incomplete biomass combustion. This decreases the apparent volatility of the particles compared to more efficiently combusted PM, where high-volatility compounds are more prevalent.[66] As shown in Figure 5 (top left), CHNO moieties (cyan) are predominantly found within SVOC and LVOC ranges,[65] reflecting their reduced volatility relative to less functionalized hydrocarbons due to the presence of oxygen- and nitrogen-containing functional groups. To capture the complete volatility distribution, average log(C_0) values were calculated across all detected fractions, including both desorbed and thermally fragmented compounds. This approach is further supported by findings indicating that organic aerosol components can undergo chemical transformations, such as decarboxylation, CO loss, and peroxide cleavage, during thermal desorption at moderate temperatures (45−100 °C).[67]

For ambient aerosols, the volatility distribution differs from both engine and RWC emissions. The elevated heteroatom content and oxidation states in both samples suggest reduced volatility, as reflected in the saturation mass concentration plot (Figure 5). SVOCs remain the dominant fraction (46−50%), while extremely low-volatility organic compounds (ELVOCs) are present at significantly higher percentages (8−12%) compared with engine and wood combustion sources. In contrast, IVOCs constitute only a minor fraction (<3%).

3.2.7. Carbon Oxidation State Trends in Organic Aerosols. The concept of carbon oxidation state (OS_C) is a key metric calculated from the elemental composition of organic aerosol (OA) to quantify its degree of oxidation and track its chemical transformation during atmospheric aging.[68]

The distributions of OS_c versus carbon number for all samples are shown in Figure 6. The shipping fuel samples

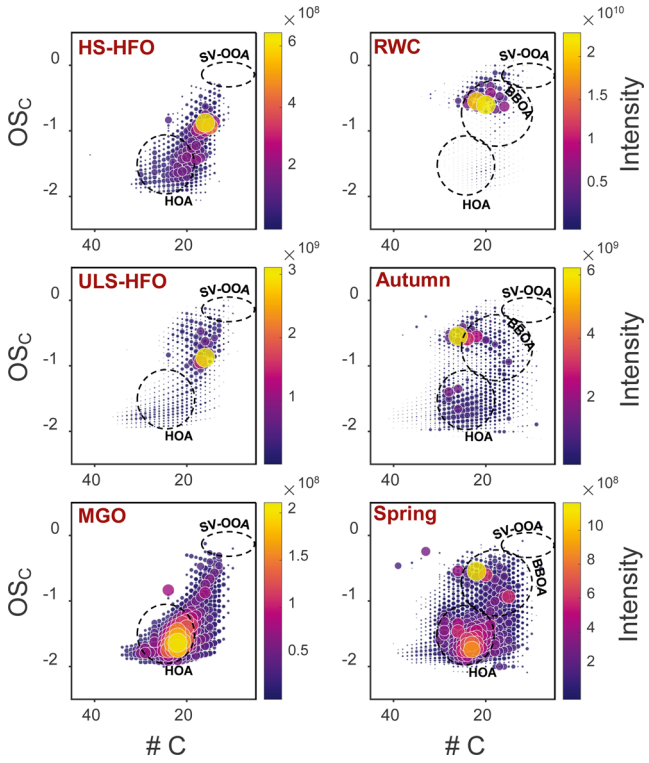

Figure 6. Average carbon oxidation state (OS_c) versus carbon number (#C) of HS-HFO 2.4%S at 60 kW, ULS-HFO 0.06%S at 60 kW, Marine Gas Oil (MGO) at 60 kW, residential wood combustion (RWC), and ambient samples, autumn and spring. Dashed black outlines denote characteristic regions for hydrocarbon-like organic aerosol (HOA), biomass burning organic aerosol (BBOA), and semivolatile oxygenated organic aerosol (SV-OOA).[68] Sum formula annotations from all OC fractions (OC1−4) are combined in this visualization.

cluster at relatively low OS_c values (−0.3 to −1.5), reflecting reduced aromatic/aliphatic species typical of hydrocarbon-like organic aerosol (HOA). Heavy fuel oils, both HS-HFO and ULS-HFO, show similar overall trends with most compounds below OS_c = 0 and concentrated at low carbon numbers (C < 20), consistent with low oxygenation and a dominance of CH-class. HS-HFO centers at $OS_c \approx -1.24$, whereas ULS-HFO shifts toward a higher average OS_c (−0.37). This indicates the enhanced formation of partially oxidized species, consistent with the DBE distribution showing PAH-like structures and oxygenated fragments (e.g., ketones, aldehydes) overlapping with the biomass burning organic aerosol (BBOA) domain. MGO displays the most reduced composition ($OS_c \approx -1.40$) across a broader range, but reflecting a simpler, less aromatic chemical space.

In contrast, RWC extends to significantly higher OS_c values (≈ -0.55), at slightly higher carbon numbers. This shift

https://doi.org/10.1021/acsmeasuresciau.5c00170
ACS Meas. Sci. Au XXXX, XXX, XXX−XXX

reflects greater aromaticity and the presence of oxygenated (CHO-class), which are absent in ship emissions, and points to incomplete combustion processes and the formation of secondary oxygenated products. The broader spread toward positive OS_c aligns with the contributions from oxygenated functional groups, including phenolics, consistent with BrC-related compounds frequently reported in biomass burning emissions.[69,70]

Ambient aerosols bridge these source profiles and, showing clear seasonal differences that support the influence of different atmospheric processes and sources on aerosol compositions. The autumn ambient sample is more oxidized, reflecting contributions from biomass burning and secondary organic aerosol (SOA) formation. In contrast, less oxidized species observed in spring likely point to a stronger influence from HOA.

4. CONCLUSION

The integration of TOCA-FT-ICR-MS represents a highly effective and versatile approach for the advanced characterization of complex carbonaceous aerosols. This analytical platform demonstrates remarkable robustness in its high-resolution mass spectrometry capabilities, successfully resolving challenging mass splits and providing precise detection of evolving species in real-time. By overcoming restrictions of traditional mass spectrometry, such as limited resolving power and mass accuracy, TOCA-APPI (+) FT-ICR-MS ensures confident molecular attribution, enabling a deeper understanding of the chemical composition of aerosol constituents.

The system's ability to keep pace with the thermal protocol enables the generation of well-defined profiles, offering deeper insights into aerosol composition. This approach facilitates the identification of organic and elemental carbon subfractions and provides insights into the structural motifs that drive combustion aerosols. Analysis of variations in aromaticity, volatility, and oxidation opens new pathways for exploring the reactivity and toxicity of aerosol components across various emission sources, including fossil fuel combustion, biomass burning, and ambient aerosols. The system consistently revealed distinct chemical fingerprints, highlighting the complexity of atmospheric particulate matter and emphasizing the influence of source-specific contributions and aging processes on aerosol composition.

Furthermore, the ability to link molecular structure with volatility and heteroatom content enhances the evaluation of the environmental and health implications of aerosols. The TOCA-FT-ICR-MS platform not only facilitates the identification of distinct compound classes and their evolution with temperature but also allows for the assignment of thousands of molecular formulas. By classifying these compounds based on their chemical characteristics and volatility, the system offers a comprehensive view of aerosol composition and transformation, establishing a solid analytical framework for future studies on atmospheric pollutants.

This approach could strengthen our understanding of emission sources, chemical aging, and their potential impacts on air quality and human health, offering valuable opportunities for regulatory assessment and source attribution, particularly in understanding both combustion-related aerosols and emerging pollutants.

ASSOCIATED CONTENT

Data Availability Statement

Data is available upon request from Christopher Rüger (christopher.rueger@uni-rostock.de).

Supporting Information

The Supporting Information is available free of charge at https://pubs.acs.org/doi/10.1021/acsmeasuresciau.5c00170.

Supporting Information (Tables S1−S5; Figures S1−S13) includes sample metadata (filter ID, emission type/source), measurement reproducibility, and TOCA carbon responses (triplicates), elemental composition-derived parameters, literature-derived compound-class coefficients, molecular property calculations, and TOCA-APPI (+) FT-ICR-MS results for engine, wood combustion, and seasonal ambient aerosols (TOCA/TIC traces, spectra, compound-class distributions/overlap, and diagnostic DBE-#C and Van Krevelen plots)-(PDF)

AUTHOR INFORMATION

Corresponding Author

Christopher Paul Rüger − *Joint Mass Spectrometry Centre (JMSC)/Chair of Analytical Chemistry, University of Rostock, Rostock 18059, Germany; Department Life, Light & Matter (LLM), University of Rostock, Rostock 18059, Germany;* orcid.org/0000-0001-9634-9239; Email: christopher.rueger@uni-rostock.de

Authors

Silvia Juliana Vesga-Martínez − *Joint Mass Spectrometry Centre (JMSC)/Chair of Analytical Chemistry, University of Rostock, Rostock 18059, Germany; Department Life, Light & Matter (LLM), University of Rostock, Rostock 18059, Germany*

Fabian Etscheidt − *Joint Mass Spectrometry Centre (JMSC)/Chair of Analytical Chemistry, University of Rostock, Rostock 18059, Germany; Photonion GmbH, Schwerin 19061, Germany*

Martin Bauer − *Joint Mass Spectrometry Centre (JMSC)/Chair of Analytical Chemistry, University of Rostock, Rostock 18059, Germany*

Patrick Martens − *University of the Bundeswehr Munich, Faculty of Mechanical Engineering, Institute of Chemistry and Environmental Engineering, Neubiberg 85577, Germany*

Anika Neumann − *Department Life, Light & Matter (LLM) and Chair of Piston Machines and Internal Combustion Engines (LKV), Faculty of Mechanical Engineering and Marine Technology, University of Rostock, Rostock 18059, Germany*

Hendryk Czech − *Joint Mass Spectrometry Centre (JMSC)/Chair of Analytical Chemistry, University of Rostock, Rostock 18059, Germany; Helmholtz Zentrum München GmbH, German Research Center for Environmental Health, Neuherberg, Germany, Cooperation group "Comprehensive Molecular Analytics" (CMA), Joint Mass Spectrometry Centre (JMSC), Munich 85764, Germany;* orcid.org/0000-0001-8377-4252

Ralf Zimmermann − *Joint Mass Spectrometry Centre (JMSC)/Chair of Analytical Chemistry, University of Rostock, Rostock 18059, Germany; Department Life, Light & Matter (LLM), University of Rostock, Rostock 18059,*

https://doi.org/10.1021/acsmeasuresciau.5c00170
ACS Meas. Sci. Au XXXX, XXX, XXX−XXX

Germany; Helmholtz Zentrum München GmbH, German Research Center for Environmental Health, Neuherberg, Germany, Cooperation group "Comprehensive Molecular Analytics" (CMA), Joint Mass Spectrometry Centre (JMSC), Munich 85764, Germany

Complete contact information is available at: https://pubs.acs.org/10.1021/acsmeasuresciau.5c00170

Author Contributions

CRediT: **Silvia Juliana Vesga-Martínez** data curation, formal analysis, investigation, validation, visualization, writing - original draft; **Christopher Paul Rüger** conceptualization, funding acquisition, methodology, project administration, software, supervision, writing - original draft; **Fabian Etscheidt** formal analysis, software, visualization, writing - review & editing; **Martin Bauer** formal analysis, investigation, software, validation, writing - review & editing; **Patrick Martens** methodology, writing - review & editing; **Anika Neumann** investigation, supervision; **Hendryk Czech** writing - review & editing; **Ralf Zimmermann** funding acquisition, project administration, resources, supervision, writing - review & editing.

Funding

Funded by the Deutsche Forschungsgemeinschaft (DFG, German Research Foundation) − 446129707. We thank the ANR (ANR-20-CE92-0036) for funding the research project TIMSAC. The authors thank the Deutsche Forschungsgemeinschaft (DFG, German Research Foundation) for funding the Bruker FT-ICR-MS (INST 264/56, 142644299).

Notes

The authors declare no competing financial interest.

■ ACKNOWLEDGMENTS

The authors thank the Interdisciplinary Faculty, Department Life, Light, and Matter at the University of Rostock for providing laboratory space and infrastructure. Consistent help and support from Aerosol d.o.o. in all matters related to the thermal-optical carbon analyzer is acknowledged. We thank Philip Jürß for careful proofreading.

■ REFERENCES

(1) Chowdhury, S.; Pozzer, A.; Haines, A.; Klingmüller, K.; Münzel, T.; Paasonen, P.; Sharma, A.; Venkataraman, C.; Lelieveld, J. Global health burden of ambient PM2.5 and the contribution of anthropogenic black carbon and organic aerosols. *Environ. Int.* **2022**, *159*, 107020.

(2) Costa, S.; Ferreira, J.; Silveira, C.; Costa, C.; Lopes, D.; Relvas, H.; Borrego, C.; Roebeling, P.; Miranda, A. I.; Teixeira, J. P. Integrating Health on Air Quality Assessment—Review Report on Health Risks of Two Major European Outdoor Air Pollutants: PM and NO_2. *J. Toxicol. Environ. Health, Part B* **2014**, *17* (6), 307−340.

(3) Cao, J.-J.; Zhu, C.-S.; Tie, X.-X.; Geng, F.-H.; Xu, H.-M.; Ho, S. S. H.; Wang, G.-H.; Han, Y.-M.; Ho, K.-F. Characteristics and sources of carbonaceous aerosols from Shanghai, China. *Atmos. Chem. Phys.* **2013**, *13*, 803−817.

(4) Diab, J.; Streibel, T.; Cavalli, F.; Lee, S. C.; Saathoff, H.; Mamakos, A.; Chow, J. C.; Chen, L.-W. A.; Watson, J. G.; Sippula, O.; Zimmermann, R. Hyphenation of a EC/OC thermal−optical carbon analyzer to photo-ionization time-of-flight mass spectrometry: an off-line aerosol mass spectrometric approach for characterization of primary and secondary particulate matter. *Atmos. Meas. Tech.* **2015**, *8*, 3337−3353.

(5) Hartner, E.; Paul, A.; Käfer, U.; Czech, H.; Hohaus, T.; Gröger, T.; Sklorz, M.; Jakobi, G.; Orasche, J.; Jeong, S.; Brejcha, R.; Ziehm, T.; Zhang, Z.-H.; Schnelle-Kreis, J.; Adam, T.; Rudich, Y.; Kiendler-Scharr, A.; Zimmermann, R. On the Complementarity and Informative Value of Different Electron Ionization Mass Spectrometric Techniques for the Chemical Analysis of Secondary Organic Aerosols. *ACS Earth Space Chem.* **2022**, *6*, 1358−1374.

(6) Castilla, C.; Rüger, C. P.; Marcotte, S.; Lavanant, H.; Afonso, C. Direct inlet probe atmospheric pressure photo and chemical ionization coupled to ultra-high resolution mass spectrometry for the description of lignocellulosic biomass. *J. Am. Soc. Mass Spectrom.* **2020**, *31*, 822−831.

(7) Castilla, C.; Rüger, C. P.; Lavanant, H.; Afonso, C. Ion mobility mass spectrometry of in situ generated biomass pyrolysis products. *J. Anal. Appl. Pyrolysis* **2021**, *156*, 105164.

(8) Rüger, C. P.; Le Maître, J.; Riches, E.; Palmer, M.; Orasche, J.; Sippula, O.; Jokiniemi, J.; Afonso, C.; Giusti, P.; Zimmermann, R. Cyclic Ion Mobility Spectrometry Coupled to High-Resolution Time-of-Flight Mass Spectrometry Equipped with Atmospheric Solid Analysis Probe for the Molecular Characterization of Combustion Particulate Matter. *J. Am. Soc. Mass Spectrom.* **2021**, *32*, 206−217.

(9) Rüger, C. P.; Tiemann, O.; Neumann, A.; Streibel, T.; Zimmermann, R. Review on Evolved Gas Analysis Mass Spectrometry with Soft Photoionization for the Chemical Description of Petroleum, Petroleum-Derived Materials, and Alternative Feedstocks. *Energy Fuels* **2021**, *35*, 18308−18332.

(10) Rüger, C. P.; Miersch, T.; Schwemer, T.; Sklorz, M.; Zimmermann, R. Hyphenation of Thermal Analysis to Ultrahigh-Resolution Mass Spectrometry (Fourier Transform Ion Cyclotron Resonance Mass Spectrometry) Using Atmospheric Pressure Chemical Ionization For Studying Composition and Thermal Degradation of Complex Materials. *Anal. Chem.* **2015**, *87*, 6493−6499.

(11) Chow, J. C.; Watson, J. G.; Chen, L. W. A.; Chang, M. C. O.; Robinson, N. F.; Trimble, D.; Kohl, S. The IMPROVE_A temperature protocol for thermal/optical carbon analysis: maintaining consistency with a long-term database. *J. Air Waste Manage. Assoc.* **2007**, *57*, 1014−1023.

(12) Grabowsky, J.; Streibel, T.; Sklorz, M.; Chow, J. C.; Watson, J. G.; Mamakos, A.; Zimmermann, R. Hyphenation of a carbon analyzer to photo-ionization mass spectrometry to unravel the organic composition of particulate matter on a molecular level. *Anal. Bioanal. Chem.* **2011**, *401*, 3153−3164.

(13) Martens, P.; Czech, H.; Orasche, J.; Abbaszade, G.; Sklorz, M.; Michalke, B.; Tissari, J.; Bizjak, T.; Ihalainen, M.; Suhonen, H.; Yli-Pirilä, P.; Jokiniemi, J.; Sippula, O.; Zimmermann, R. Brown Coal and Logwood Combustion in a Modern Heating Appliance: The Impact of Combustion Quality and Fuel on Organic Aerosol Composition. *Environ. Sci. Technol.* **2023**, *57*, 5532−5543.

(14) Etscheidt, F.; Rüger, C. P.; Schwarz, C.; Tiemann, O.; Neumann, A.; Hansen, H. J.; Streibel, T.; Ehlert, S.; Zimmermann, R. Atmospheric Pressure Laser Ionization Mass Spectrometry with Tunable UV Wavelength Utilizing an Optical Parametric Oscillator. *Anal. Chem.* **2025**, *97*, 676−685.

(15) Neumann, A.; Tiemann, O.; Hansen, H. J.; Rüger, C. P.; Zimmermann, R. Detailed Comparison of Xenon APPI (9.6/8.4 eV), Krypton APPI (10.6/10.0 eV), APCI, and APLI (266 nm) for Gas Chromatography High Resolution Mass Spectrometry of Standards and Complex Mixtures. *J. Am. Soc. Mass Spectrom.* **2023**, *34*, 1632−1646.

(16) Rüger, C. P.; Neumann, A.; Sklorz, M.; Zimmermann, R. Atmospheric Pressure Single Photon Laser Ionization (APSPLI) Mass Spectrometry Using a 157 nm Fluorine Excimer Laser for Sensitive and Selective Detection of Non- to Semipolar Hydrocarbons. *Anal. Chem.* **2021**, *93*, 3691−3697.

(17) Rossner, A.; Farant, J. P.; Simon, P.; Wick, D. P. Development of a flow controller for long-term sampling of gases and vapors using evacuated canisters. *Environ. Sci. Technol.* **2002**, *36*, 4912−4920.

(18) Rüger, C. P.; Neumann, A.; Sklorz, M.; Schwemer, T.; Zimmermann, R. Thermal Analysis Coupled to Ultrahigh Resolution Mass Spectrometry with Collision Induced Dissociation for Complex Petroleum Samples: Heavy Oil Composition and Asphaltene Precipitation Effects. *Energy Fuels* **2017**, *31*, 13144−13158.
(19) Rüger, C. P.; Schwemer, T.; Sklorz, M.; O'Connor, P. B.; Barrow, M. P.; Zimmermann, R. Comprehensive chemical comparison of fuel composition and aerosol particles emitted from a ship diesel engine by gas chromatography atmospheric pressure chemical ionisation ultra-high resolution mass spectrometry with improved data processing routines. *Eur. J. Mass Spectrom.* **2017**, *23*, 28−39.
(20) Delistraty, D. Toxic equivalency factor approach for risk assessment of polycyclic aromatic hydrocarbons. *Toxicol. Environ. Chem.* **1997**, *64*, 81−108.
(21) Kauppila, T. J.; Syage, J. A.; Benter, T. Recent developments in atmospheric pressure photoionization-mass spectrometry. *Mass Spectrom. Rev.* **2017**, *36*, 423−449.
(22) Mase, C.; Maillard, J. F.; Piparo, M.; Friederici, L.; Rüger, C. P.; Marceau, S.; Paupy, B.; Hubert-Roux, M.; Afonso, C.; Giusti, P. GC-FTICR mass spectrometry with dopant assisted atmospheric pressure photoionization: application to the characterization of plastic pyrolysis oil. *Analyst* **2023**, *148*, 5221−5232.
(23) Byer, J. D.; Siek, K.; Jobst, K. Distinguishing the C3 vs SH4Mass Split by Comprehensive Two-Dimensional Gas Chromatography-High Resolution Time-of-Flight Mass Spectrometry. *Anal. Chem.* **2016**, *88*, 6101−6104.
(24) Rüger, C. P.; Sklorz, M.; Schwemer, T.; Zimmermann, R. Characterisation of ship diesel primary particulate matter at the molecular level by means of ultra-high-resolution mass spectrometry coupled to laser desorption ionisation−comparison of feed fuel, filter extracts and direct particle measurements. *Anal. Bioanal. Chem.* **2015**, *407*, 5923−5937.
(25) Schneider, E.; Czech, H.; Hansen, H. J.; Jeong, S.; Bendl, J.; Saraji-Bozorgzad, M.; Sklorz, M.; Etzien, U.; Buchholz, B.; Streibel, T.; Adam, T. W.; Rüger, C. P.; Zimmermann, R. Humic-like Substances (HULIS) in Ship Engine Emissions: Molecular Composition Effected by Fuel Type, Engine Mode, and Wet Scrubber Usage. *Environ. Sci. Technol.* **2023**, *57*, 13948−13958.
(26) Purcell, J. M.; Hendrickson, C. L.; Rodgers, R. P.; Marshall, A. G. Atmospheric pressure photoionization fourier transform ion cyclotron resonance mass spectrometry for complex mixture analysis. *Anal. Chem.* **2006**, *78*, 5906−5912.
(27) Jeong, S.; Bendl, J.; Saraji-Bozorgzad, M.; Käfer, U.; Etzien, U.; Schade, J.; Bauer, M.; Jakobi, G.; Orasche, J.; Fisch, K.; Cwierz, P. P.; Rüger, C. P.; Czech, H.; Karg, E.; Heyen, G.; Krausnick, M.; Geissler, A.; Geipel, C.; Streibel, T.; Schnelle-Kreis, J.; Sklorz, M.; Schulz-Bull, D. E.; Buchholz, B.; Adam, T.; Zimmermann, R. Aerosol emissions from a marine diesel engine running on different fuels and effects of exhaust gas cleaning measures. *Environ. Pollut.* **2023**, *316*, 120526.
(28) Jeong, S.; Pantzke, J.; Offer, S.; Käfer, U.; Bendl, J.; Saraji-Bozorgzad, M.; Huber, A.; Michalke, B.; Etzien, U.; Jakobi, G.; Orasche, J.; Czech, H.; Rüger, C. P.; Schnelle-Kreis, J.; Streibel, T.; Buchholz, B.; Adam, T.; Sklorz, M.; Di Bucchianico, S.; Zimmermann, R. In vitro genotoxic and mutagenic potentials of combustion particles from marine fuels with different sulfur contents. *Environ. Int.* **2025**, *198*, 109440.
(29) Momenimovahed, A.; Gagné, S.; Martens, P.; Jakobi, G.; Czech, H.; Wichmann, V.; Buchholz, B.; Zimmermann, R.; Behrends, B.; Thomson, K. A. Comparison of black carbon measurement techniques for marine engine emissions using three marine fuel types. *Aerosol Sci. Technol.* **2022**, *56*, 46−62.
(30) Streibel, T.; Schnelle-Kreis, J.; Czech, H.; Harndorf, H.; Jakobi, G.; Jokiniemi, J.; Karg, E.; Lintelmann, J.; Matuschek, G.; Michalke, B.; Müller, L.; Orasche, J.; Passig, J.; Radischat, C.; Rabe, R.; Reda, A.; Rüger, C.; Schwemer, T.; Sippula, O.; Stengel, B.; Sklorz, M.; Torvela, T.; Weggler, B.; Zimmermann, R. Aerosol emissions of a ship diesel engine operated with diesel fuel or heavy fuel oil. *Environ. Sci. Pollut. Res. Int.* **2017**, *24*, 10976−10991.
(31) Lacroix-Andrivet, O.; Castilla, C.; Rüger, C.; Hubert-Roux, M.; Mendes Siqueira, A. L.; Giusti, P.; Afonso, C. Direct Insertion Analysis of Polymer-Modified Bitumen by Atmospheric Pressure Chemical Ionization Ultrahigh-Resolution Mass Spectrometry. *Energy Fuels* **2021**, *35*, 2165−2173.
(32) Tose, L. V.; Murgu, M.; Vaz, B. G.; Romão, W. Application of Atmospheric Solids Analysis Probe Mass Spectrometry (ASAP-MS) in Petroleomics: Analysis of Condensed Aromatics Standards, Crude Oil, and Paraffinic Fraction. *J. Am. Soc. Mass Spectrom.* **2017**, *28*, 2401−2407.
(33) Schneider, E.; Czech, H.; Popovicheva, O.; Chichaeva, M.; Kobelev, V.; Kasimov, N.; Minkina, T.; Rüger, C. P.; Zimmermann, R. Mass spectrometric analysis of unprecedented high levels of carbonaceous aerosol particles long-range transported from wildfires in the Siberian Arctic. *Atmos. Chem. Phys.* **2024**, *24*, 553−576.
(34) Chow, J. C.; Riggio, G. M.; Wang, X.; Chen, L.-W. A.; Watson, J. G. Measuring the Organic Carbon to Organic Matter Multiplier with Thermal/Optical Carbon-Quadrupole Mass Spectrometer Analyses. *Aerosol Sci. Eng.* **2018**, *2*, 165−172.
(35) McIver, R. T. Trajectory calculations for axial injection of ions into a magnetic field: overcoming the magnetic mirror effect with an r.f. quadrupole lens. *Int. J. Mass Spectrom. Ion Processes* **1990**, *98*, 35−50.
(36) Wanczek, K. P.; Kanawati, B. FT-ICR mass spectrometry: Superconducting magnet, external ion source, ion−molecule reactions, and ion-ion traps. *Mass Spectrom. Rev.* **2022**, *41*, 338−351.
(37) Rüger, C. P.; Grimmer, C.; Sklorz, M.; Neumann, A.; Streibel, T.; Zimmermann, R. Combination of Different Thermal Analysis Methods Coupled to Mass Spectrometry for the Analysis of Asphaltenes and Their Parent Crude Oils: Comprehensive Characterization of the Molecular Pyrolysis Pattern. *Energy Fuels* **2018**, *32*, 2699−2711.
(38) Kösling, P.; Rüger, C. P.; Schade, J.; Ehlert, S.; Etzien, U.; Kozhinov, A. N.; Tsybin, Y. O.; Rigler, M.; Adam, T.; Walte, A.; Buchholz, B.; Zimmermann, R. Real-Time Investigation of Primary Ship Engine Emissions by Vacuum Resonance-Enhanced Multiphoton Ionization High-Resolution Orbitrap Mass Spectrometry. *Anal. Chem.* **2022**, *94*, 16855−16863.
(39) Degrendele, C.; Kanduč, T.; Kocman, D.; Lammel, G.; Cambelová, A.; Dos Santos, S. G.; Horvat, M.; Kukučka, P.; Holubová Šmejkalová, A.; Mikeš, O.; Nuñez-Corcuera, B.; Přibylová, P.; Prokeš, R.; Saňka, O.; Maggos, T.; Sarigiannis, D.; Klánová, J. NPAHs and OPAHs in the atmosphere of two central European cities: Seasonality, urban-to-background gradients, cancer risks and gas-to-particle partitioning. *Sci. Total Environ.* **2021**, *793*, 148528.
(40) Kitanovski, Z.; Shahpoury, P.; Samara, C.; Voliotis, A.; Lammel, G. Composition and mass size distribution of nitrated and oxygenated aromatic compounds in ambient particulate matter from southern and central Europe − implications for the origin. *Atmos. Chem. Phys.* **2020**, *20*, 2471−2487.
(41) Tsiodra, I.; Grivas, G.; Bougiatioti, A.; Tavernaraki, K.; Parinos, C.; Paraskevopoulou, D.; Papoutsidaki, K.; Tsagkaraki, M.; Kozonaki, F.-A.; Oikonomou, K.; Nenes, A.; Mihalopoulos, N. Source apportionment of particle-bound polycyclic aromatic hydrocarbons (PAHs), oxygenated PAHs (OPAHs), and their associated long-term health risks in a major European city. *Sci. Total Environ.* **2024**, *951*, 175416.
(42) Shen, R.; Schäfer, K.; Schnelle-Kreis, J.; Shao, L.; Norra, S.; Kramar, U.; Michalke, B.; Abbaszade, G.; Streibel, T.; Fricker, M.; Chen, Y.; Zimmermann, R.; Emeis, S.; Schmid, H. P. Characteristics and sources of PM in seasonal perspective − A case study from one year continuously sampling in Beijing. *Atmos. Pollut. Res.* **2016**, *7*, 235−248.
(43) Shen, R.; Schäfer, K.; Schnelle-Kreis, J.; Shao, L.; Norra, S.; Kramar, U.; Michalke, B.; Abbaszade, G.; Streibel, T.; Zimmermann, R.; Emeis, S. Seasonal variability and source distribution of haze particles from a continuous one-year study in Beijing. *Atmos. Pollut. Res.* **2018**, *9*, 627−633.

https://doi.org/10.1021/acsmeasuresciau.5c00170
ACS Meas. Sci. Au XXXX, XXX, XXX−XXX

(44) Elmquist, M.; Cornelissen, G.; Kukulska, Z.; Gustafsson, Ö. Distinct oxidative stabilities of char versus soot black carbon: Implications for quantification and environmental recalcitrance. *Global Biogeochem. Cycles* **2006**, *20*, 2005GB002629.
(45) Fernandes, M. B.; Skjemstad, J. O.; Johnson, B. B.; Wells, J. D.; Brooks, P. Characterization of carbonaceous combustion residues. I. Morphological, elemental and spectroscopic features. *Chemosphere* **2003**, *51*, 785−795.
(46) Dzepina, K.; Arey, J.; Marr, L. C.; Worsnop, D. R.; Salcedo, D.; Zhang, Q.; Onasch, T. B.; Molina, L. T.; Molina, M. J.; Jimenez, J. L. Detection of particle-phase polycyclic aromatic hydrocarbons in Mexico City using an aerosol mass spectrometer. *Int. J. Mass Spectrom.* **2007**, *263*, 152−170.
(47) Zhang, J.; Li, K.; Wang, T.; Gammelsæter, E.; Cheung, R. K. Y.; Surdu, M.; Bogler, S.; Bhattu, D.; Wang, D. S.; Cui, T.; Qi, L.; Lamkaddam, H.; El Haddad, I.; Slowik, J. G.; Prevot, A. S. H.; Bell, D. M. Bulk and molecular-level composition of primary organic aerosol from wood, straw, cow dung, and plastic burning. *Atmos. Chem. Phys.* **2023**, *23*, 14561−14576.
(48) Cheng, Y.; Duan, F.; He, K.; Zheng, M.; Du, Z.; Ma, Y.; Tan, J. Intercomparison of thermal-optical methods for the determination of organic and elemental carbon: influences of aerosol composition and implications. *Environ. Sci. Technol.* **2011**, *45*, 10117−10123.
(49) Chow, J. C.; Watson, J. G.; Lu, Z.; Lowenthal, D. H.; Frazier, C. A.; Solomon, P. A.; Thuillier, R. H.; Magliano, K. Descriptive analysis of PM2.5 and PM10 at regionally representative locations during SJVAQS/AUSPEX. *Atmos. Environ.* **1996**, *30*, 2079−2112.
(50) Sandrini, S.; Fuzzi, S.; Piazzalunga, A.; Prati, P.; Bonasoni, P.; Cavalli, F.; Bove, M. C.; Calvello, M.; Cappelletti, D.; Colombi, C.; et al. Spatial and seasonal variability of carbonaceous aerosol across Italy. *Atmos. Environ.* **2014**, *99*, 587−598.
(51) Chacón-Patiño, M. L.; Rowland, S. M.; Rodgers, R. P. Advances in Asphaltene Petroleomics. Part 1: Asphaltenes Are Composed of Abundant Island and Archipelago Structural Motifs. *Energy Fuels* **2017**, *31*, 13509−13518.
(52) Neumann, A.; Chacón-Patiño, M. L.; Rodgers, R. P.; Rüger, C. P.; Zimmermann, R. Investigation of Island/Single-Core- and Archipelago/Multicore-Enriched Asphaltenes and Their Solubility Fractions by Thermal Analysis Coupled with High-Resolution Fourier Transform Ion Cyclotron Resonance Mass Spectrometry. *Energy Fuels* **2021**, *35*, 3808−3824.
(53) Rüger, C. P.; Neumann, A.; Kösling, P.; Vesga Martínez, S. J.; Chacón-Patiño, M. L.; Rodgers, R. P.; Zimmermann, R. Addressing Thermal Behavior and Molecular Architecture of Asphaltenes by a Thermal-Optical Carbon Analyzer Coupled to High-Resolution Mass Spectrometry. *Energy Fuels* **2022**, *36*, 10177−10190.
(54) Mueller, L.; Jakobi, G.; Czech, H.; Stengel, B.; Orasche, J.; Arteaga-Salas, J. M.; Karg, E.; Elsasser, M.; Sippula, O.; Streibel, T.; Slowik, J. G.; Prevot, A. S.; Jokiniemi, J.; Rabe, R.; Harndorf, H.; Michalke, B.; Schnelle-Kreis, J.; Zimmermann, R. Characteristics and temporal evolution of particulate emissions from a ship diesel engine. *Appl. Energy* **2015**, *155*, 204−217.
(55) Liu, X.; Wang, H.; Wang, F.; Lv, S.; Wu, C.; Zhao, Y.; Zhang, S.; Liu, S.; Xu, X.; Lei, Y.; Wang, G. Secondary Formation of Atmospheric Brown Carbon in China Haze: Implication for an Enhancing Role of Ammonia. *Environ. Sci. Technol.* **2023**, *57*, 11163−11172.
(56) Iakovides, M.; Iakovides, G.; Stephanou, E. G. Atmospheric particle-bound polycyclic aromatic hydrocarbons, n-alkanes, hopanes, steranes and trace metals: PM2.5 source identification, individual and cumulative multi-pathway lifetime cancer risk assessment in the urban environment. *Sci. Total Environ.* **2021**, *752*, 141834.
(57) Worton, D. R.; Isaacman, G.; Gentner, D. R.; Dallmann, T. R.; Chan, A. W. H.; Ruehl, C.; Kirchstetter, T. W.; Wilson, K. R.; Harley, R. A.; Goldstein, A. H. Lubricating oil dominates primary organic aerosol emissions from motor vehicles. *Environ. Sci. Technol.* **2014**, *48*, 3698−3706.
(58) Ma, J.; Reininger, N.; Zhao, C.; Döbler, D.; Rüdiger, J.; Qiu, Y.; Ungeheuer, F.; Simon, M.; D'Angelo, L.; Breuninger, A.; David, J.; Bai, Y.; Li, Y.; Xue, Y.; Li, L.; Wang, Y.; Hildmann, S.; Hoffmann, T.; Liu, B.; Niu, H.; Wu, Z.; Vogel, A. L. Unveiling a large fraction of hidden organosulfates in ambient organic aerosol. *Nat. Commun.* **2025**, *16*, 4098.
(59) Yang, Y.; Chu, M.; Jia, C.; Zhou, L.; Sun, X.; Gao, M. The Partitional Behavior of sulfur and minerals in the thermal fragmentation char during pyrolysis of lignite. *Fuel* **2022**, *308*, 121954.
(60) Fan, W.; Chen, T.; Zhu, Z.; Zhang, H.; Qiu, Y.; Yin, D. A review of secondary organic aerosols formation focusing on organosulfates and organic nitrates. *J. Hazard. Mater.* **2022**, *430*, 128406.
(61) Salvador, C. M. G.; Tang, R.; Priestley, M.; Li, L.; Tsiligiannis, E.; Le Breton, M.; Zhu, W.; Zeng, L.; Wang, H.; Yu, Y.; Hu, M.; Guo, S.; Hallquist, M. Ambient nitro-aromatic compounds − biomass burning versus secondary formation in rural China. *Atmos. Chem. Phys.* **2021**, *21*, 1389−1406.
(62) Lin, P.; Aiona, P. K.; Li, Y.; Shiraiwa, M.; Laskin, J.; Nizkorodov, S. A.; Laskin, A. Molecular Characterization of Brown Carbon in Biomass Burning Aerosol Particles. *Environ. Sci. Technol.* **2016**, *50*, 11815−11824.
(63) Xie, M.; Chen, X.; Hays, M. D.; Lewandowski, M.; Offenberg, J.; Kleindienst, T. E.; Holder, A. L. Light Absorption of Secondary Organic Aerosol: Composition and Contribution of Nitroaromatic Compounds. *Environ. Sci. Technol.* **2017**, *51*, 11607−11616.
(64) Zhang, T.; Shen, Z.; Zeng, Y.; Cheng, C.; Wang, D.; Zhang, Q.; Lei, Y.; Zhang, Y.; Sun, J.; Xu, H.; Ho, S. S. H.; Cao, J. Light absorption properties and molecular profiles of HULIS in PM2.5 emitted from biomass burning in traditional "Heated Kang" in Northwest China. *Sci. Total Environ.* **2021**, *776*, 146014.
(65) Li, Y.; Pöschl, U.; Shiraiwa, M. Molecular corridors and parameterizations of volatility in the chemical evolution of organic aerosols. *Atmos. Chem. Phys.* **2016**, *16*, 3327−3344.
(66) Czech, H.; Miersch, T.; Orasche, J.; Abbaszade, G.; Sippula, O.; Tissari, J.; Michalke, B.; Schnelle-Kreis, J.; Streibel, T.; Jokiniemi, J.; Zimmermann, R. Chemical composition and speciation of particulate organic matter from modern residential small-scale wood combustion appliances. *Sci. Total Environ.* **2018**, *612*, 636−648.
(67) Zhao, Z.; Yang, X.; Lee, J.; Tolentino, R.; Mayorga, R.; Zhang, W.; Zhang, H. Diverse Reactions in Highly Functionalized Organic Aerosols during Thermal Desorption. *ACS Earth Space Chem.* **2020**, *4*, 283−296.
(68) Kroll, J. H.; Donahue, N. M.; Jimenez, J. L.; Kessler, S. H.; Canagaratna, M. R.; Wilson, K. R.; Altieri, K. E.; Mazzoleni, L. R.; Wozniak, A. S.; Bluhm, H.; Mysak, E. R.; Smith, J. D.; Kolb, C. E.; Worsnop, D. R. Carbon oxidation state as a metric for describing the chemistry of atmospheric organic aerosol. *Nat. Chem.* **2011**, *3*, 133−139.
(69) Oghama, O. E.; Voliotis, A.; Bannan, T. J.; Syafira, S. A.; Hu, D.; Wu, H.; Gallimore, P.; McFiggans, G.; Coe, H.; Allan, J. D. Variations in oxygenated and nitrogen-containing primary organic compounds based on the fuel type and burning condition in stove emissions. *Environ. Sci.: Atmos.* **2025**, *5*, 1297.
(70) Tang, J.; Li, J.; Su, T.; Han, Y.; Mo, Y.; Jiang, H.; Cui, M.; Jiang, B.; Chen, Y.; Tang, J.; Song, J.; Peng, P.; Zhang, G. Molecular compositions and optical properties of dissolved brown carbon in biomass burning, coal combustion, and vehicle emission aerosols illuminated by excitation−emission matrix spectroscopy and Fourier transform ion cyclotron resonance mass spectrometry analysis. *Atmos. Chem. Phys.* **2020**, *20*, 2513−2532.

https://doi.org/10.1021/acsmeasuresciau.5c00170
ACS Meas. Sci. Au XXXX, XXX, XXX−XXX